H-Ras activation and fibroblast-associated TGF-β signaling promote laminin-332 accumulation and invasion in cutaneous squamous cell carcinoma

Elina Siljamäki[1,2], Pekka Rappu[1,2], Pilvi Riihilä[1,3,4], Liisa Nissinen [1,3,4], Veli-Matti Kähäri[1,3,4] and Jyrki Heino[1,2*]

[1] MediCity Research Laboratory, University of Turku, Tykistökatu 6A, 20520, Turku, Finland

[2] Department of Biochemistry, University of Turku, Tykistökatu 6A, 20520, Turku, Finland

[3] Department of Dermatology, University of Turku and Turku University Hospital, Kiinamyllynkatu 10, 20520, Turku, Finland

[4] The Western Cancer Centre of the Cancer Centre Finland (FICAN West), University of Turku and Turku University Hospital, Kiinamyllynkatu 10, 20520, Turku, Finland

Elina Siljamäki, elisil@utu.fi
Pekka Rappu, pekrappu@utu.fi
Pilvi Riihilä, pimati@utu.fi
Liisa Nissinen, liinis@utu.fi
Veli-Matti Kähäri, velkah@utu.fi
*Jyrki Heino, jyrki.heino@utu.fi

***Corresponding Author**
Jyrki Heino, M.D., Ph.D.,
Department of Biochemistry
FI-20014 University of Turku, Turku, Finland
Phone: +358-50-5238351
E-mail: jyrki.heino@utu.fi

ABBREVIATIONS

α-SMA, α-smooth muscle actin

BM, basement membrane

cSCC, cutaneous squamous cell carcinoma

DMSO, dimethyl sulfoxide

ECM, extracellular matrix

EGF, epidermal growth factor

EGFR, epidermal growth factor receptor

FCS, fetal calf serum

FGF-2, fibroblast growth factor-2

H-Ras, Harvey rat sarcoma viral oncogene homolog

IFN-γ, interferon-γ

IGF-I, insulin-like growth factor-I

IHC, immunohistochemistry

IL-1β, interleukin-1β

KGF, keratinocyte growth factor

LAMA3, laminin subunit alpha 3

LAMB3, laminin subunit beta 3

LAMC2, laminin subunit gamma 2

PI3K, phosphatidylinositol 3-kinase

TGF-α, transforming growth factor-α

TGF-β, transforming growth factor-β

TMA, tissue microarray

TNF-α, tumor necrosis factor-α

VEGF, vascular endothelial growth factor

ABSTRACT

Cutaneous squamous cell carcinoma (cSCC) is the most common metastatic skin cancer, with increasing incidence worldwide. The molecular basis of cSCC progression to invasive and metastatic disease is still incompletely understood. Here, we show that fibroblasts and transforming growth factor-β (TGF-β) signaling promotes laminin-332 accumulation in cancer cells in an activated H-Ras-dependent manner, which in turn promotes cancer cell invasion. Immunohistochemical analysis of sporadic UV-induced invasive human cSCCs (n=208) revealed prominent cSCC cell specific immunostaining for laminin-332 γ2 chain, located in the majority of cases (90%, n=173) in the invasive edge of the tumors. To mimic the progression of cSCC we established 3D spheroid cocultures using primary skin fibroblasts and HaCaT/*ras*-HaCaT human keratinocytes. Our results indicate that in 3D spheroids, unlike in monolayer cultures, TGF-β upregulates laminin-332 production, but only in cells that harbour oncogenic H-Ras. Accumulation of laminin-332 was prevented by both H-Ras knock down and inhibition of TGF-β signaling by SB431542 or RAdKD-ALK5 kinase-defective adenovirus. Furthermore, fibroblasts accelerated the invasion of *ras*-HaCaT cells through collagen I gels in a Ras/TGF-β signaling dependent manner. In conclusion, we demonstrate the presence of laminin-332 in the invasive front of cSCC tumors and report a new Ras/TGF-β-dependent mechanism that promotes laminin-332 accumulation and cancer cell invasion.

Keywords: cSCC / fibroblast / H-Ras / invasion / laminin-332 / TGF-β

INTRODUCTION

Cutaneous squamous cell carcinoma (cSCC) is the most common metastatic skin cancer, with increasing incidence worldwide [1], [2]. cSCC progresses from premalignant lesion, actinic keratosis, to carcinoma *in situ* (cSCCIS) and finally to invasive and metastatic disease [2]. The molecular basis of cSCC progression is incompletely understood, but activating mutations in *HRAS*, *KRAS* and epidermal growth factor receptor (*EGFR*) have been found [3], [4]. Previously, it has been suggested that PI3K signaling pathway participates in the cSCC progression. Ras signaling alone, however, was not found to be sufficient to activate PI3K/AKT pathway in cSCC tumors, and therefore it was speculated that signals from the tumor stroma may also be needed for PI3K activation and subsequent cSCC tumorigenesis [5].

Tumor stroma, or tumor microenvironment, is a complex meshwork of extracellular matrix (ECM), activated fibroblasts, immune cells and capillary vessels [6]. Currently, indisputable evidence show that cancer progression is not led solely by cancer cells but that the tumor microenvironment plays a critical role in the development of aberrant tissue functions and malignancies [7], [8]. In this microenvironment, fibroblasts are the most abundant cell type, and by producing soluble proteins, such as growth factors and various ECM components they control the behaviour of other cell types. Recently, numerous studies have shown that fibroblasts have a significant functional role in nearly all aspects of tumor progression. They promote tumor growth and invasion, induce angiogenesis, modulate inflammation and promote chemoresistance [9], [10], [11].

In the past few years, three-dimensional (3D) cell cultures have gained increasing interest while the limitations of traditional two-dimensional (2D) monolayer cell cultures have been recognized. The cells in monolayer cultures cannot form the same natural organization as the cells *in vivo* in a tissue, in which all cells are surrounded by other cells or the ECM. Spheroids provide more tissue-like environment, which enables the cellular interactions that are vital for the natural function of the cells. In addition to close cell–cell/cell–ECM interactions, spheroids of cancer cells also limit oxygen and nutrition flow into the cells resulting in different populations of proliferating, quiescent

and necrotic cells [12]. Because of these features cancer cell spheroids resemble solid tumors and can serve as an *in vitro* model to better mimic the *in vivo* tumor tissue properties.

In the present study, we show how fibroblasts modify ECM expression in tumor-like 3D spheroids and how they influence on cancer cell invasion. First, we observed that in cSCC tumor samples laminin-332 is frequently produced by cancer cells located in the invasive front. To study this further we used HaCaT/*ras*-HaCaT human keratinocyte carcinogenesis model which mimics the progression of cSCC [13]. Our data indicate that when cocultured together with fibroblasts, the transformed epithelial cells show increased invasive capacity and they also produce high levels of laminin-332. The invasion and the increase in laminin-332 production are shown to require concomitant activation of H-Ras and TGF-β signaling pathways in cancer cells. These results unveil a molecular mechanism that explains the high level of laminin-332 in human cSCC tumors, which in turn promotes cancer cell invasion.

RESULTS

Laminin γ2 is accumulated in the invasive edge in cSCC tumors

Immunohistochemical analyses have revealed high laminin-332 γ2 chain accumulation in cSCC, and also its increased production in pre-malignant conditions, such as actinic keratosis and cSCCIS [14], [15]. To investigate the localisation of laminin-332 γ2 chain in more detail, we analysed with immunohistochemistry (IHC) a large panel of sporadic UV-induced invasive cSCCs (n=208) in tissue microarrays (TMA). Prominent tumor cell-specific immunostaining of laminin γ2 was noted in cSCC tumor cell cytoplasm (Fig. 1A, Supplementary Fig. 1A). Moreover, in the majority of cases (90%, n=173) the positive staining of laminin γ2 was noted in the invasive edge of cSCC tumors (Fig. 1A, blow-up image). The staining intensity of laminin γ2 was analysed and scored as negative, weak, moderate or strong (Fig. 1B). In 56% of the cSCC sections this semiquantitative analysis showed strong staining (Fig. 1B) whereas the staining intensity was scored as negative in 6% of cases only. In addition, staining with α-smooth muscle actin antibody (α-SMA) showed that activated stromal fibroblasts did not express laminin γ2 (Supplementary Fig. 1A). To conclude, these results demonstrate marked accumulation of laminin-332 γ2 chain in tumor cells but not in stromal fibroblasts. The fact that the strongest accumulation was most often detected in the invasive front suggests a role for laminin in the cell migration and also proposes that tumor cell–fibroblast interaction plays a role in the production of laminin by the cancer cells. In general the findings are in agreement with previous results suggesting that laminin-332 accumulation correlates with invasiveness and poor prognosis in many cancers, including cSCC [16], [17], [18].

Malignant transformation or Ras activation alone are not sufficient to induce laminin-332 accumulation

As we detected strong accumulation of laminin-332 γ2 chain in the cSCC tumor cells, we next analysed laminin-332 levels in four primary and three metastatic cSCC cell lines that were cultured as 3D spheroids, which imitate more accurately the *in vivo* conditions compared to the traditional 2D

cell cultures. The spheroids were grown for five days, after which the accumulation of laminin-332 was analysed by Western blotting. The results indicated that all seven cSCC cell lines produced detectable levels of laminin-332, but a prominent overexpression was detected only in a metastatic cell line, UT-SCC-115 (Fig. 1C). Thus, the induction of laminin-332 synthesis was less abundant in cSCC derived cell lines than in tumors. Interestingly, UT-SCC-115 was also the only cSCC cell line that showed a potent activation of extracellular signal-regulated kinase 1/2 (ERK1/2) phosphorylation (Fig. 1C), suggesting a connection between the activation of mitogenic ERK1/2 pathway and laminin-332 production. Approximately 11% of cSCCs harbour an activating mutation in *RAS* gene [3], [19], but most probably there are also other cancer related mechanisms, which activate ERK1/2 phosphorylation.

To study the putative connection between Ras signaling/mitogen-activated protein kinase (MAPK) activation and laminin-332 accumulation in cSCC, we used the HaCaT/*ras*-HaCaT human keratinocyte carcinogenesis model, which is a well-established tool for exploring the progression of cSCC from benign lesions to malignant tumors [13]. The model utilises spontaneously immortalized, non-tumorigenic human keratinocyte cell line, HaCaT, and its three retrovirally H-Ras-transformed subclones, A5, II-4 and RT3 (abbreviated as *ras*-HaCaT cells in the text) that exhibit benign, invasive and metastatic phenotypes, respectively, after subcutaneous injection into athymic nude mice [13], [20], [21]. *Ras*-HaCaT cells have been shown to express high levels of phosphorylated ERK1/2 [22], and also here, when cultured as spheroids all three cell lines harbouring H-Ras showed remarkably increased ERK1/2 phosphorylation when compared to HaCaT cells (Fig. 1D and Supplementary Fig. 1B). However, the accumulation of laminin-332 into the spheroids was only slightly elevated (Fig. 1D), and in repeated experiments the differences did not reach statistical significance (Supplementary Fig. 1B). Thus, the activation of Ras/ERK pathway alone did not explain the overexpression of laminin-332 seen in cSCC tumors.

Figure 1

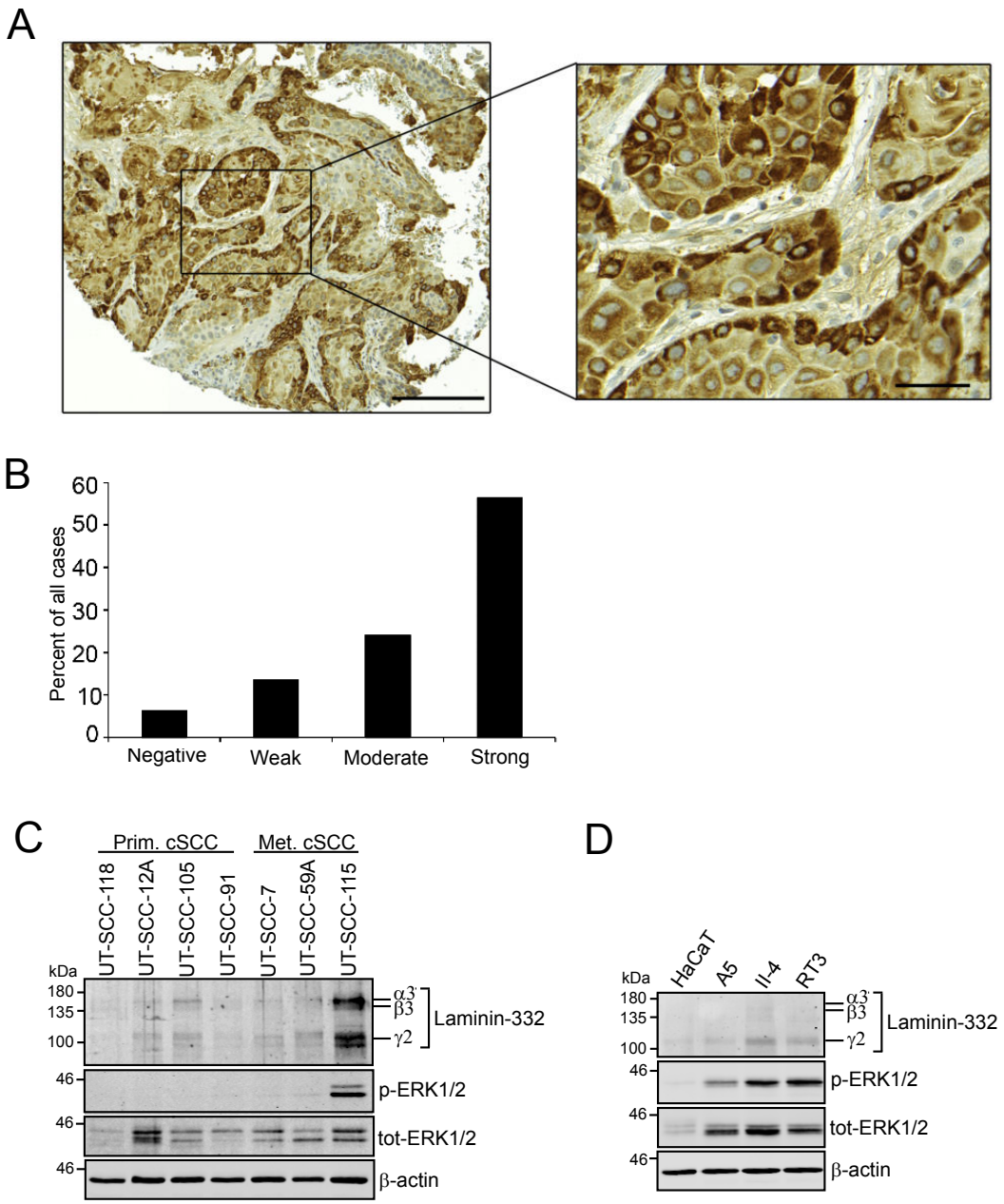

Figure 1. Laminin-332 in cutaneous squamous cell carcinoma (cSCC). (A) Tissue microarray sections of UV-induced sporadic cSCCs (n=208) were stained with laminin γ2 antibody. Strong cytoplasmic staining of laminin γ2 in cSCC cells was noted in the invasive edge of tumors (blow-up image). Scale bar in lower magnification is 200 μm and in higher magnification 50 μm. (B) The immunostaining of laminin γ2 was scored as negative, weak, moderate or strong, based on the specific cytoplasmic staining intensity of cSCC tumor cells. (C) Four primary and three metastatic cSCC cell lines were cultured as 3D spheroids for five days, and the levels of laminin-332, phosphorylated ERK1/2 (p-ERK1/2) and total ERK1/2 (tot-ERK1/2) were analysed by Western blotting. β-actin was used as a loading control. (C) Non-tumorigenic HaCaT and H-Ras-transformed HaCaT cells (A5, II-4 and RT3, *i.e. ras*-HaCaT cells) were cultured as 3D spheroids for five days, and the levels of laminin-332, p-ERK1/2 and tot-ERK1/2 were analysed by Western blotting. β-actin was used as a loading control. Representative Western blots from three independent biological replicates are shown.

Fibroblasts induce laminin-332 production in H-Ras-transformed HaCaT keratinocytes

To study the role of fibroblast–cancer cell interaction in the regulation of laminin-332 production in conditions that reflect the native architecture of actual tumors, we established spheroid type cocultures of primary human skin fibroblasts together with either HaCaT cell line or one of the three *ras*-HaCaT clones, *i.e.* A5, II-4 and RT3.

At first, to characterize the localization of different cell lines in our 3D spheroids, we labeled the cells in monolayer cultures with CellTrackers (fibroblasts with green and HaCaT/*ras*-HaCaT cells with red tracker) and after that, cocultured them as spheroids for five days. Confocal imaging revealed peripheral localization of fibroblasts (in 95% of the samples, n=20) when they were cocultured with non-tumorigenic HaCaT cells, which in turn were located in the core of the spheroid (Fig. 2A). Cocultures with benign A5 cells showed more heterogeneity, as in 58% of the spheroids fibroblasts located in the outer shell of the spheroid (n=24; p=0.006, Fisher's exact test). On the contrary, the outer shell was conquered by invasive II-4 cells (81%; n=21; p=7.2e-07, Fisher's exact test) or with metastatic RT3 cells (77%; n=22; p=1.6e-06, Fisher's exact test) when they were cultured with fibroblasts (Fig. 2A). The localization of H-Ras-transformed II-4 and RT3 cells in the outermost surface of the spheroid most likely reflects their invasive and metastatic potentials. These results thus confirmed that we had successfully created a 3D cell coculture model, where the epithelial cells and fibroblasts are localized differentially in the spheroids, depending on the invasive potential of the HaCaT/*ras*-HaCaT cell line.

Next, we used a mass spectrometry method to unveil the core matrisome in similar 3D coculture spheroids that were used for confocal imaging. In addition, we cultured fibroblasts and HaCaT/*ras*-HaCaT cells alone as spheroids. A quantitative proteomics analysis showed that fibroblasts produced almost entirely the main structural components of the core matrisome (Supplementary Fig. 2 and Supplementary Data 1). In cocultures marked changes were seen in the accumulation of *LAMA3* (α3), *LAMC2* (γ2) and *LAMB3* (β3) chains only. Their expression was enhanced in spheroids that contained fibroblasts together with II-4 or RT3 cells, when compared to

spheroids that encompassed HaCaT or A5 cells with fibroblasts (Fig. 2B). All the single cell type spheroids showed only a moderate expression of *LAMA3*, *LAMC2* and *LAMB3* genes (Fig. 2B), indicating that the increase in cocultured II-4 and RT3 spheroids was dependent on the presence of fibroblasts. The mass spectrometry results were confirmed by Western blot analysis, which showed that in the spheroids, laminin-332 amount increases along invasive and metastatic potential of the cells, when HaCaT, A5, II-4 or RT3 cells are cultured together with fibroblasts (Fig. 2C and Supplementary Fig. 3).

In order to examine which cell type possess the observed increase in laminin-332 accumulation (*i.e*. whether fibroblasts induce HaCaT/*ras*-HaCaT cells to produce laminin-332 or vice versa), confocal imaging was performed. The results showed that laminin-332 is produced by the parental HaCaT and *ras*-HaCaT cells (Fig. 2D), confirming the results of IHC stainings of cSCC tumors, which showed laminin-332 γ2 chain accumulation in tumor cells and not in fibroblasts (Supplementary Fig. 1A). Confocal imaging results were verified by a computational analysis method that allowed us to analyse the expression profiles of the spheroids by taking into account different diameters and the intensity values of the spheroids. The expression profile of RT3 cells cultured together with fibroblasts showed the most prominent laminin-332 expression arising in the edges of the spheroid, where also RT3 cells reside (Fig. 2E).

In conclusion, our results show that fibroblasts stimulate laminin-332 production in the H-Ras-transformed HaCaT cell lines and that the laminin-332 levels correlate with the invasion capacity.

Figure 2

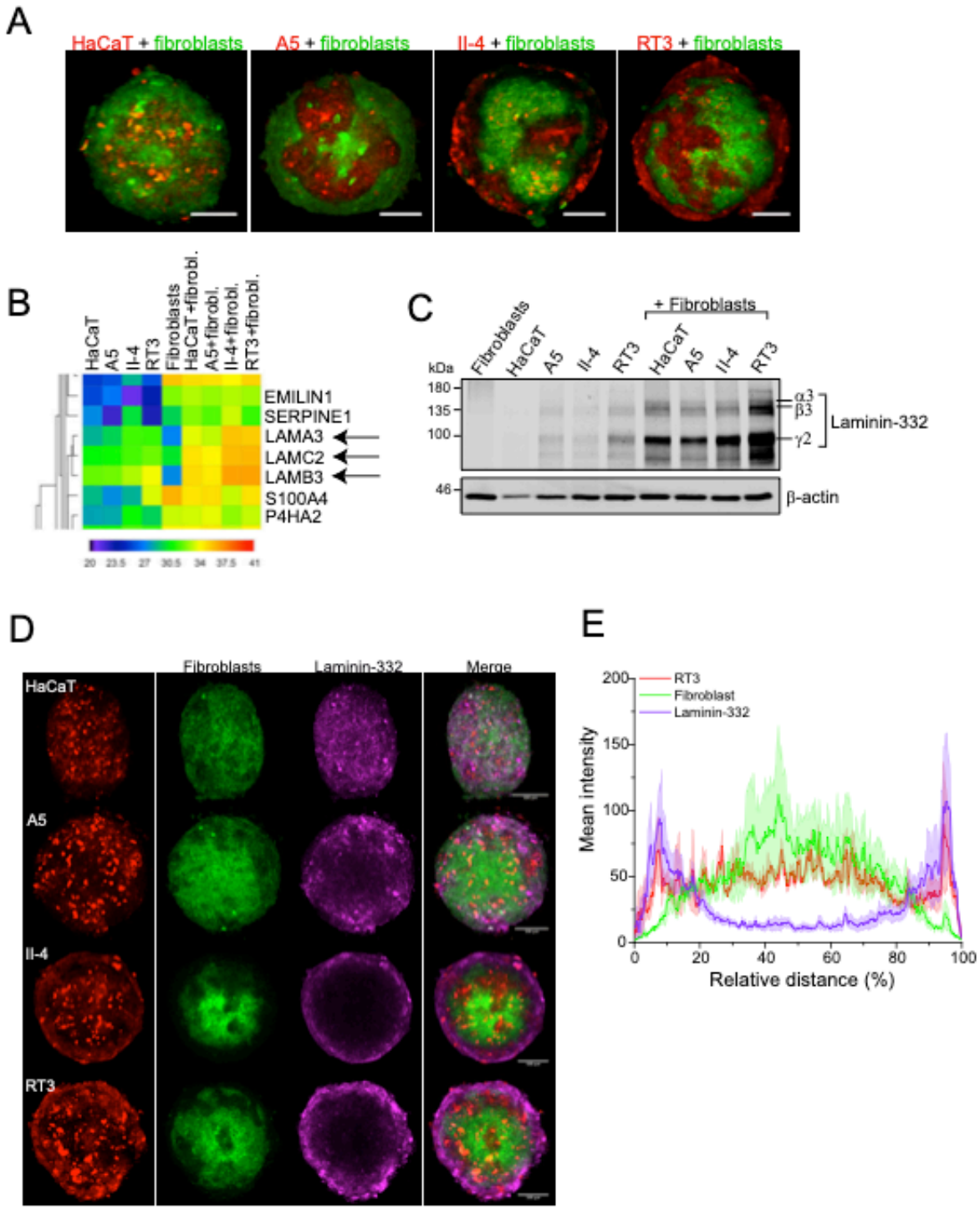

164 **Figure 2.** Fibroblasts induce cancer cells to produce laminin-332. (A) Confocal images of non-tumorigenic
165 HaCaT and *ras*-HaCaT cells (A5, II-4 and RT3) in five-day-old 3D spheroids with skin primary fibroblasts.
166 The cells were labeled with CellTrackers (HaCaT/*ras*-HaCaT cells in red and fibroblasts in green). Scale bar,
167 500 μm. Three independent biological replicates were performed. HaCaT/fibroblasts, n=20; A5/fibroblasts,
168 n=24; II-4/fibroblasts, n=21; RT3/fibroblasts, n=22. (B) Mass spectrometric analysis of HaCaT/*ras*-HaCaT
169 cells in 3D spheroids, cultured with or without skin primary fibroblasts. The arrows point to *LAMA3*, *LAMC2*
170 and *LAMB3* genes, which together form laminin-332. (C) Western blot analysis of HaCaT/*ras*-HaCaT cells in
171 3D spheroids cultured with or without skin primary fibroblasts. The expression of α3, β3 and γ2 chains of
172 laminin-332 are shown. β-actin was used as a loading control. Representative Western blots from four
173 independent biological replicates are shown. (D) Confocal images of 3D HaCaT/*ras*-HaCaT cells cultured
174 with skin primary fibroblasts. The cells were first labeled with CellTrackers (HaCaT/*ras*-HaCaT cells in red

and fibroblasts in green) and the spheroids were allowed to grow for five days. After PFA fixation, the spheroids were subjected to immunofluorescence and stained for laminin-332. Scale bar, 500 μm. Three independent biological replicates were performed. HaCaT/fibroblasts, n=11; A5/fibroblasts, n=13; II-4/fibroblasts, n=12; RT3/fibroblasts, n=12. (E) The expression profile of 3D spheroids containing RT3 cells and skin primary fibroblasts. The cells were treated as in (D), and the expression profile was calculated from the confocal images. Mean intensity values show the intensities of RT3 cells (red), fibroblasts (green) and laminin-332 (magenta), and relative distance indicates the diameter of the spheroids. 12 spheroids from three biological replicates were analysed. Mean (dark line) ± S.E.M. (light area around the line) is shown.

H-Ras silencing decreases laminin-332 synthesis in 3D spheroids but not in 2D monolayer cultures

We next examined the connection between laminin-332 production and Ras signaling in the 3D spheroid model by silencing H-Ras from parental HaCaT and H-Ras-transformed A5, II-4 and RT3 cell lines. First, H-Ras was silenced with a specific siRNA in 2D monolayer cell cultures for 24h, followed by 3D spheroid formation with fibroblasts. The spheroids were then allowed to grow for five days before harvesting for Western blotting. The analysis showed that H-Ras silencing decreased laminin-332 α3, β3 and γ2 chain synthesis in all three cell lines expressing the oncogenic H-Ras (Fig. 3A and Supplementary Fig. 4A). The functionality of H-Ras silencing was confirmed by blotting the samples for phosphorylated ERK1/2 (Fig. 3A). In spheroids containing a single cell type, HaCaT, A5 or II-4, only faint laminin-332 production was detected, and knock down of H-Ras had no effect. Spheroids containing solely RT3 cells showed higher levels of laminin-332, and its production was also decreased by H-Ras silencing (Fig. 3B and Supplementary Fig. 4B), whereas when H-Ras was depleted in RT3 cells in monolayers, laminin-332 synthesis was not altered (Fig. 3C and Supplementary Fig. 4C). To conclude, our results show that H-Ras silencing decreases laminin-332 synthesis in 3D spheroid, but not in 2D monolayer cultures. As the abnormal cell morphology in 2D cell cultures is known to affect gene and protein expression [23], [24], our findings also highlight the benefits of 3D cultures when cellular interactions in tumors are studied.

Figure 3

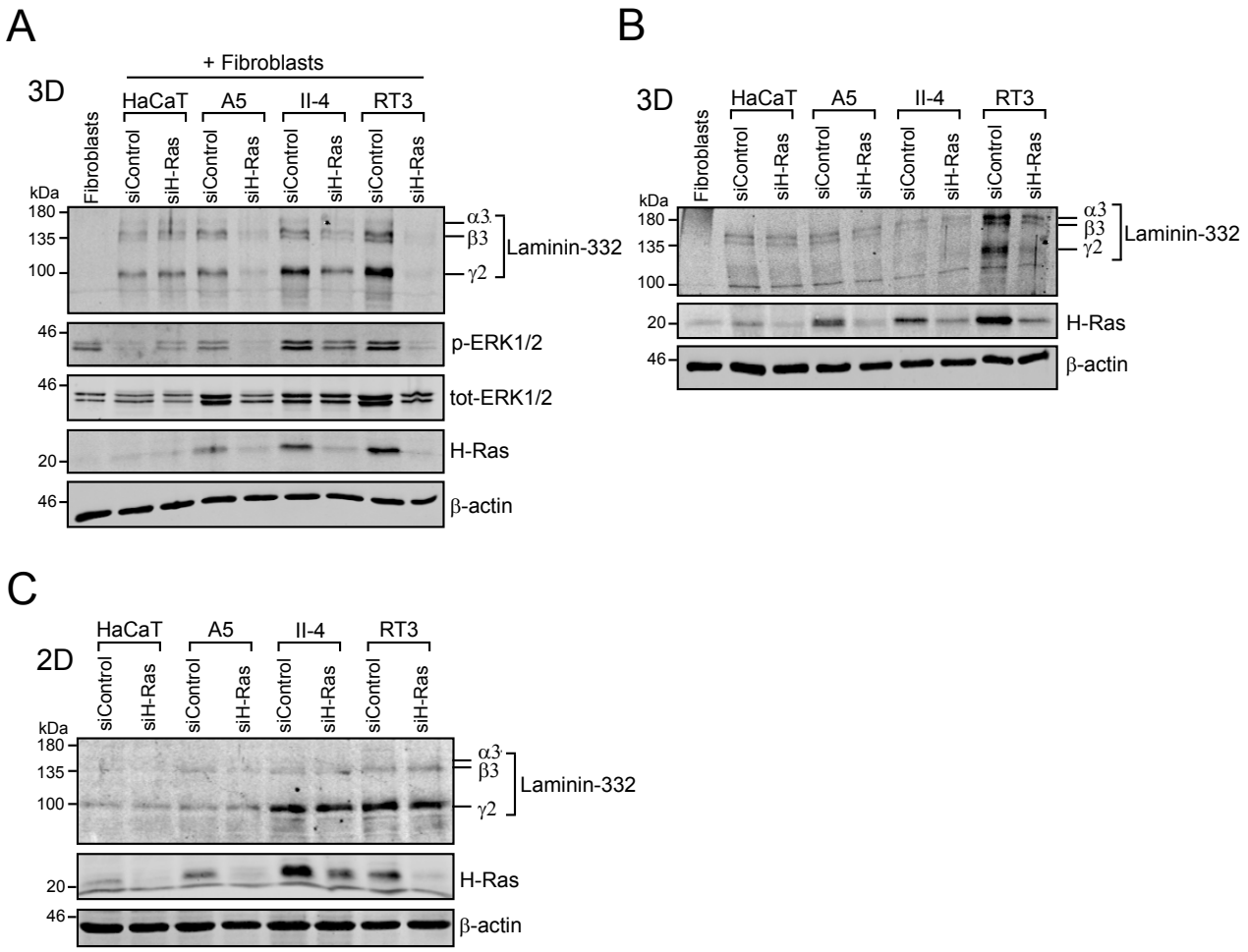

Figure 3. H-Ras silencing decreases laminin-332 synthesis in 3D spheroids. (A) Western blot analysis of 3D cultured HaCaT/*ras*-HaCaT cells with skin primary fibroblasts. Before spheroid formation, H-Ras was silenced in HaCaT/*ras*-HaCaT cells for 24h. The spheroids were then allowed to grow for five days and harvested for Western blot analysis. β-actin was used as a loading control. Representative Western blots from three independent biological replicates are shown. (B) Western blot analysis of five-day-old 3D cultured fibroblasts and HaCaT/*ras*-HaCaT cells. H-Ras was silenced in HaCaT/*ras*-HaCaT cells for 24h before spheroid formation. β-actin was used as a loading control. Representative Western blots from three independent biological replicates are shown. (C) Western blot analysis of 2D cultured HaCaT/*ras*-HaCaT cells. H-Ras was silenced for 72h before harvesting the cells for Western blotting. β-actin was used as a loading control. Representative Western blots from three independent biological replicates are shown.

TGF-β enhances laminin-332 production in cells harbouring active H-Ras

Next, we further studied our observation that laminin-332 accumulation in RT3 cells requires a close contact to fibroblasts, in addition to the active H-Ras signaling and 3D cell culture conditions. Fibroblasts have been reported to regulate cancer cells by secretion of soluble factors, e.g. growth factors [25]. To test this possibility in our experimental model, RT3 cells were cultured in spheroids for 24h and treated with a panel of growth factors and cytokines for additional 48h. Western blotting showed that TGF-β treatment (5 ng/ml) resulted in a strong increase in laminin-332 production, while a less potent upregulation was also seen by tumor necrosis factor-α (TNF-α) and epidermal growth factor (EGF) (Fig. 4A). In HaCaT cells only the EGF treatment generated an increase in laminin-332 production (Supplementary Fig. 5A), which suggests that EGF signaling, possibly through Ras/MAPK pathway, is able to increase laminin-332 synthesis in non-tumorigenic HaCaT cells.

These results encouraged us to concentrate on TGF-β signaling as a potent fibroblast-derived signaling pathway that could co-operate with H-Ras signaling to induce laminin-332 synthesis. We therefore inhibited TGF-β signaling by using SB431542, a specific inhibitor of TGF-β type I receptor kinase activity (inhibitor of ALK4/5/7). At first, we confirmed the functionality of SB431542 by treating HaCaT and RT3 cells with the inhibitor (10 μM) for 24h, followed by TGF-β-treatment (10 ng/ml, 30 min in +37°C). SB431542 inhibited Smad2 phosphorylation completely both in HaCaT and RT3 cells, indicating that it was able to repress the TGFβ1/Smad2 signaling (Fig. 4B). We next treated HaCaT and RT3 cells with the inhibitor for 24h, followed by spheroid formation together with fibroblasts. The spheroids were allowed to grow for five days. Western blotting showed that when RT3 cells were treated with the inhibitor, fibroblasts were no longer able to induce laminin-332 synthesis when compared to the spheroids that were treated with the solvent dimethyl sulfoxide (DMSO) only (Fig. 4C and Supplementary Fig. 5B). The fact that HaCaT cells do not express large amounts of laminin-332 with or without fibroblasts (Fig. 3A, B) was also obvious in the experiments with SB431542 (Fig. 4C). When RT3 cells were treated with the inhibitor and cultured as spheroids without fibroblasts, only the amount of γ2 chain was decreased significantly (Supplementary Fig. 5C,

D). This suggests that without externally added TGF-β, only laminin-332 γ2 chain is regulated by TGF-β signaling pathway. To confirm the observation that the increase in laminin-332 production in RT3 cells is dependent on fibroblast-derived TGF-β signaling, we used adenoviral vector coding for kinase-defective ALK5 (RAdKD-ALK5) or empty vector (RAd66) as a control. RT3 cells were either left uninfected or infected for 72h with RAdKD-ALK5 or with RAd66. Expression of RAdKD-ALK5 markedly suppressed TGF-β-induced Smad2 phosphorylation when compared to control samples, confirming that the kinase-defective adenovirus was able to inhibit TGF-β signaling (Supplementary Fig. 5E). We next infected RT3 cells with RAdKD-ALK5 or RAd66 adenoviruses for 24h and after that, spheroids were allowed to form with fibroblasts for 72h. Western blot analysis showed that the fibroblasts failed to increase laminin-332 synthesis in RT3 cells infected with kinase-defective RAdKD-ALK5 (Fig. 4D and Supplementary Fig. 5F). Thus, the results supported the hypothesis that TGF-β signaling in RT3 cells is essential for the induction of laminin-332 production by fibroblasts. Our results show that in RT3 cells increase in laminin-332 production requires both TGF-β- and Ras-activated signaling pathways. H-Ras-transformed HaCaT cells can produce TGF-β, but still fibroblast-related factors drastically increased laminin-332 production. Fibroblasts can contribute in the process in two different mechanisms. Firstly, they can produce TGF-β and simply increase the local concentration of this growth factor [26]. Secondly, TGF-β is produced as an inactive precursor [27] and fibroblasts are often required for TGF-β activation via a complex process involving fibroblast-derived ECM proteins and RGD-motif binding integrins [28], [29].

Figure 4

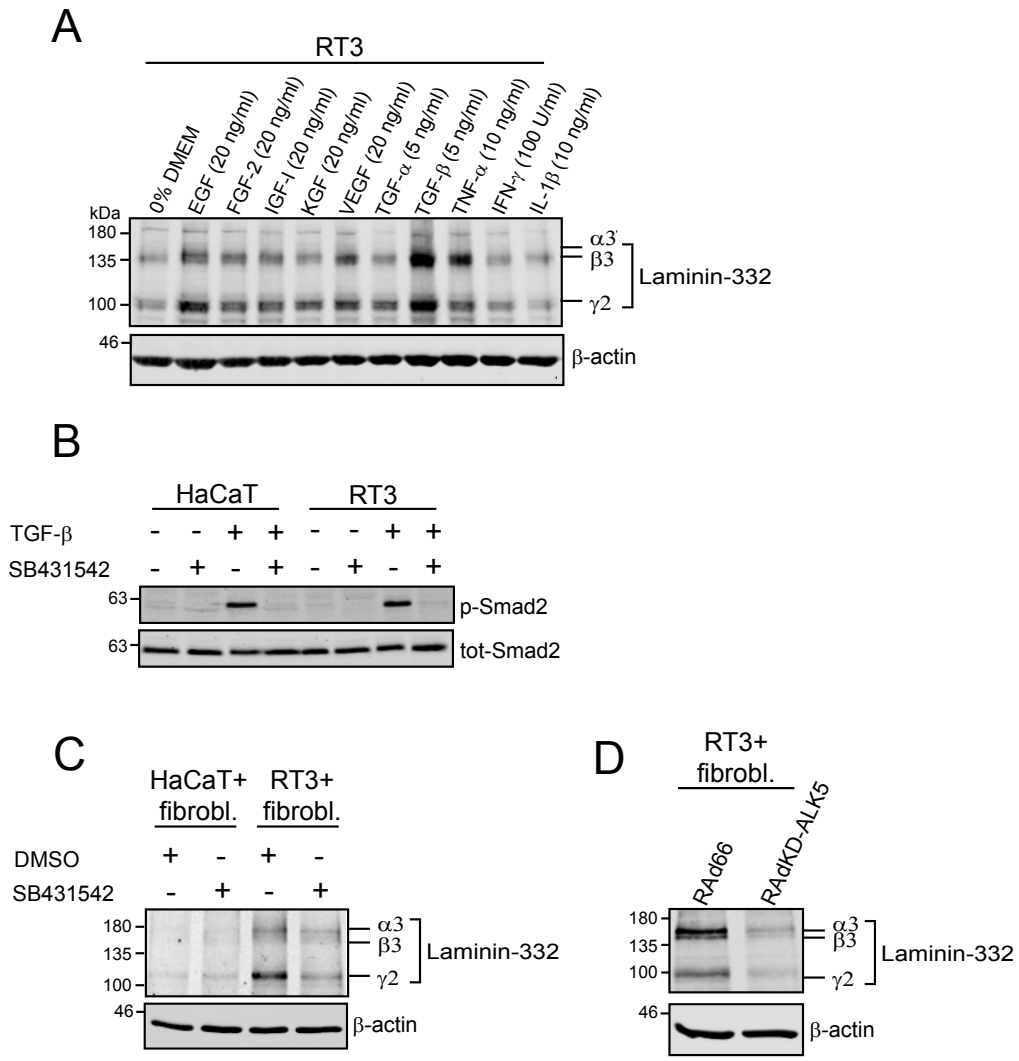

Figure 4. TGF-β enhances laminin-332 production in cells harbouring active H-Ras. (A) Western blot analysis of RT3 cells that were grown as 3D spheroids for three days. The spheroids were then subjected to panel of growth factors and cytokines (epidermal growth factor (EGF); fibroblast growth factor-2 (FGF-2); insulin-like growth factor-I (IGF-I); keratinocyte growth factor (KGF); vascular endothelial growth factor (VEGF); transforming growth factor-α (TGF-α); transforming growth factor-β (TGF-β); tumor necrosis factor-α (TNF-α); interferon-γ (IFN-γ) and interleukin-1β (IL-1β)) for additional 48h. β-actin was used as a loading control. (B) HaCaT and RT3 cells were grown in 2D conditions and treated with SB431542 for 24h. After that, the cells were stimulated with TGF-β (10 ng/ml) for 30 min. Phosphorylated Smad2 (p-Smad2) and total Smad2 (tot-Smad2) levels were analysed by Western blotting. (C) HaCaT and RT3 cells were treated with SB431542 for 24h, followed by 3D spheroid formation with skin primary fibroblasts. The spheroids were allowed to grow for five days before harvesting for Western blotting. β-actin was used as a loading control. Representative Western blots from three independent biological replicates are shown. (D) RT3 cells were infected (100 MOI) with control virus RAd66 or with adenovirus coding for kinase-defective ALK5 (RAdKD-ALK5) for 24h, followed by 3D spheroid formation with skin primary fibroblasts. After three days, the spheroids were harvested and analysed by Western blotting. β-actin was used as a loading control. Representative Western blots from three independent biological replicates are shown.

Fibroblasts promote RT3 cell invasion through collagen I in a H-Ras-dependent manner

In the immunohistochemical analysis of the cSCC tumors we observed strong accumulation of laminin-332 in the invasive front, which suggested that laminin promotes the invasive behaviour of the cancer cells. Furthermore, the aberrant activation of Ras proteins and the consequent activation of MAPKs is known to regulate virtually all aspects of cancer progression, including cell proliferation, invasion and metastasis [30], [31]. Therefore, we tested here whether H-Ras silencing affects cell invasion out of spheroids into collagen I gels. H-Ras was first silenced in HaCaT or RT3 cells for 24h in monolayer cultures, after which the cells were stained with CellTrackers (HaCaT and RT3 cells with red, fibroblasts with green) followed by spheroid formation with or without fibroblasts. Three-day-old spheroids were then embedded in collagen I and the invasion (measured as the diameter of the area covered by cells) was followed by confocal imaging for every 24h during five days. The images showed that non-tumorigenic HaCaT cells did not invade out of fibroblast-containing spheroids (Fig. 5A, C). In contrast, the fibroblasts significantly promoted invasion by the metastatic RT3 cell line, and the invasion was totally abolished by siRNAs knocking down H-Ras (Fig. 5B, C). Notably, RT3 cells did not invade at all out of spheroids containing this cell type alone (Fig. 5C and Supplementary Fig. 6A). Thus, the RT3 cell invasion through collagen I was entirely dependent on fibroblasts. The invasion of fibroblasts out of HaCaT/fibroblast or RT3/fibroblast coculture spheroids was not affected by H-Ras silencing (Fig. 5D). Thus, the inhibition of cell invasion by H-Ras knock down was cancer cell specific. Taken together, our data show that fibroblasts are indispensable for RT3 cell invasion, and that this is mediated via oncogenic H-Ras.

Fibroblasts induce RT3 cell invasion through collagen I in a TGF-β-dependent manner

To test whether TGF-β1 signaling would also affect cell invasion, we treated RT3 cells with SB431542 for 24h prior to spheroid formation with or without fibroblasts. Three-day-old spheroids were embedded in collagen I and the invasion was followed by confocal microscope every 24h during five days. Treatment with SB431542 significantly decreased RT3 cell invasion out of coculture

298 spheroids when compared to DMSO treated control samples (Fig. 5E and Supplementary Fig. 6B),

299 while fibroblast invasion was not affected by SB431542 treatment of the RT3 cells (Fig. 5F).

Figure 5

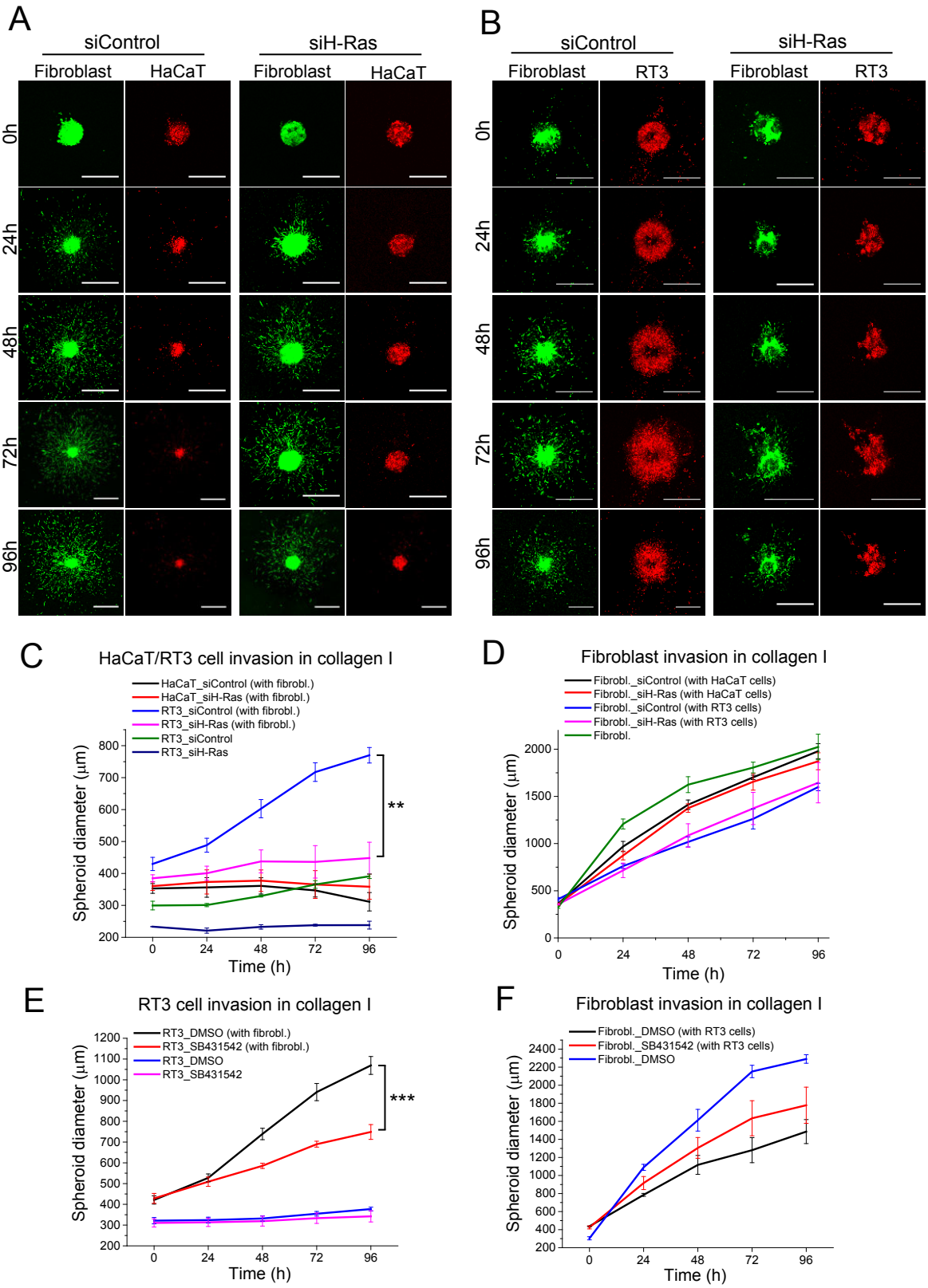

300 **Figure 5.** Fibroblasts promote RT3 cell invasion through collagen I in a H-Ras- and TGF-β-dependent manner.
301 (A, B) HaCaT cells (A) or RT3 cells (B) were first silenced with H-Ras siRNA for 24h, the spheroids were
302 then formed with skin primary fibroblasts and allowed to grow for three days. After that, the spheroids were

transferred to a 96-well plate and embedded with a collagen I gel. The invasion was followed by a confocal microscope every 24h during five days. Scale bar, 500 μm. From each time point, 2-4 spheroids were imaged and analysed. Three independent biological replicates were performed. (C) Analysis of HaCaT and RT3 cell invasion from cocultured or monocultured (RT3 cells only) spheroids that were treated as in (A) and (B). The graph shows mean from three independent biological replicates ± S.E.M. (Each replicate contained 2-4 spheroids). $^{**}p < 0.01$; one-way ANOVA followed by Tukey post hoc test. (D) Analysis of fibroblast invasion from cocultured spheroids that were treated as in (A) and (B). The graph shows mean from three independent biological replicates ± S.E.M. (Each replicate contained 2-4 spheroids). (E) Analysis of RT3 cell invasion from cocultured or monocultured (RT3 cells only) 3D spheroids. RT3 cells were first treated with SB431542 or DMSO for 24h, the spheroids were then formed with or without skin primary fibroblasts and allowed to grow for three days. After that, the spheroids were transferred to a 96-well plate and embedded with a collagen I gel. The invasion was followed every 24h for five days. The graph shows mean from three independent biological replicates ± S.E.M. (Each replicate contained 2-4 spheroids). $^{***}p < 0.001$; one-way ANOVA followed by Tukey post hoc test. (F) Analysis of fibroblast invasion from cocultured or monocultured (fibroblasts only) 3D spheroids. The spheroids were made and treated as in (E). The graph shows mean from three independent biological replicates ± S.E.M. (Each replicate contained 2-4 spheroids).

Inhibition of laminin-332 synthesis and blocking its binding to cellular receptor decrease RT3 cell invasion through collagen I

To confirm the important role of laminin-332 in cSCC invasion, we silenced laminin-332 α3, β3 and γ2 chains by using specific siRNAs against each chain. RT3 cells were treated with siRNAs in 2D monolayer cell cultures for 24h, followed by spheroid formation together with skin primary fibroblasts. After three days, the spheroids were transferred to 96-well plates and embedded in collagen I for invasion assays. The siRNAs silenced the production of their target proteins by 70-80% (Fig. 6A, B). As shown in Fig. 6C, laminin-332 depletion significantly decreased RT3 cell invasion when compared to control siRNA treated cells, whereas fibroblast invasion was not affected (Fig. 6D).

In keratinocytes, α6β4 integrin is the main receptor for laminin-332 [32]. In hemidesmosomes, integrin α6β4 anchors cells to the basement membrane [33], however, the same receptor promotes cell invasion in cancer [34], [35], [36]. To study further the role of laminin-332 in cancer cell invasion, we carried out invasion assays in the presence of function-blocking antibody against α6 integrin subunit. RT3 cells were detached from cell culture plastic in 2D condition, incubated with blocking α6 integrin antibody (40 μg/ml) for 1h/+37°C, followed by spheroid formation with skin primary fibroblasts. After three days, the spheroids were transferred to a 96-well plate and embedded in collagen I for invasion assays. Confocal images of the spheroids showed that

RT3 cells treated with blocking α6 integrin antibody were not able to invade as efficiently as control cells that were treated with normal rat IgG (Fig. 6E). When compared to the IgG control, there was a significant decrease in RT3 cell invasion in the presence of α6 integrin antibody (Fig. 6F). Fibroblast invasion however was not affected by α6 integrin blocking (Fig. 6G). Altogether, these results demonstrate the important role of laminin-332 in cancer cell invasion, since both laminin-332 knock down and blocking of its binding to cellular receptor significantly decreased RT3 cell invasion.

Figure 6

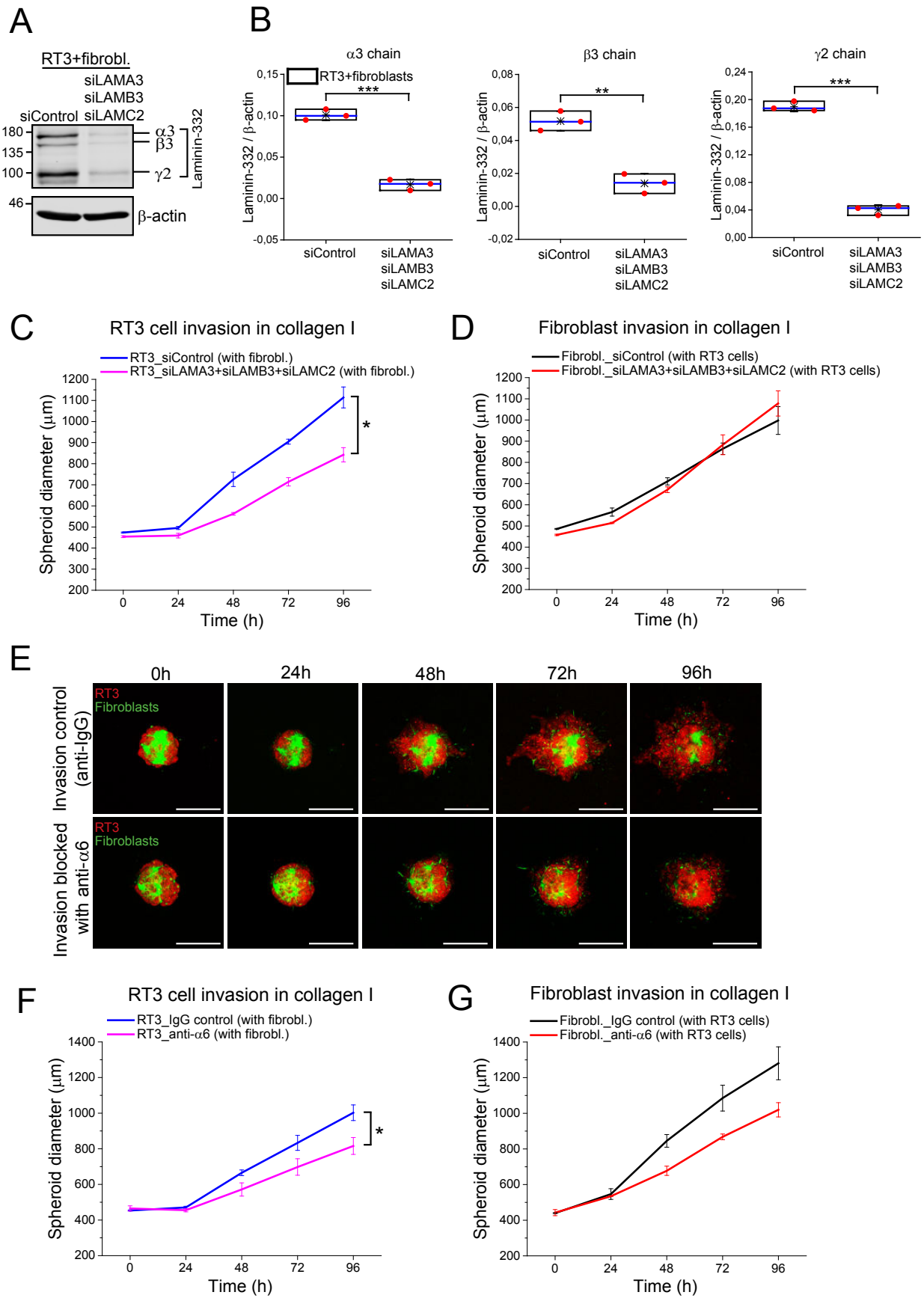

Figure 6. Laminin-332 silencing and α6 integrin blocking decrease RT3 cell invasion through collagen I. (A) Western blot analysis of 3D cultured RT3 cells with skin primary fibroblasts. Before spheroid formation, laminin-332 α3, β3 and γ2 chains (LAMA3, LAMB3 and LAMC2, respectively) were silenced in RT3 cells for 24h. The spheroids were then allowed to grow for three days and harvested for Western blot analysis. β-

actin was used as a loading control. Representative Western blots from three independent biological replicates are shown. (B) Quantification of α3, β3 and γ2 chain levels from Western blots in Figure 6A. Box plots show data from three independent biological replicates (red dots), the second and third quartiles (the box), the median (blue line) and the mean (star) from all experiments ± S.D. ***p<0.001, **p<0.01 (Student's t-test). (C) Analysis of RT3 cell invasion through collagen I. RT3 cells were first silenced with control siRNA or LAMA3, LAMB3 and LAMC2 siRNAs for 24h, the spheroids were then formed with skin primary fibroblasts and allowed to grow for three days. After that, the spheroids were transferred to a 96-well plate and embedded in a collagen I gel. The invasion was followed for five days. The graph shows mean from three independent biological replicates ± S.E.M. (Each replicate contained 2-4 spheroids). *p<0.05 (Student's t-test). (D) Analysis of fibroblast invasion from the same 3D spheroids as in (*C*). The graph shows mean from three independent biological replicates ± S.E.M. (Each replicate contained 2-4 spheroids). (D) RT3 cells were treated with α6 integrin blocking antibody (40 μg/ml) or as a control, with normal rat IgG (40 μg/ml) for 1h/+37°C, following spheroid formation with skin primary fibroblasts. The spheroids were then allowed to grow for three days. After that, the spheroids were transferred to a 96-well plate and embedded in a collagen I gel. The invasion was followed by a confocal microscope every 24h during five days. Scale bar, 500 μm. (E) Analysis of RT3 cell invasion through collagen I. The coculture spheroids with fibroblasts were made as described in (*D*). The graph shows mean from three independent biological replicates ± S.E.M. (Each replicate contained 2-4 spheroids). *p<0.05 (Student's t-test). (F) Analysis of fibroblast invasion from the same 3D spheroids as in (*E*). The graph shows mean from three independent biological replicates ± S.E.M. (Each replicate contained 2-4 spheroids).

TGF-β and MAPK signaling pathways are coactivated *in vivo* in conjunction with increased laminin-332 levels

Finally, to get *in vivo* support for our hypothesis that TGF-β and MAPK signaling pathways collaborate in laminin-332 regulation, we analysed the production of laminin γ2 chain, p-Smad2 and p-ERK1/2 in a panel of sporadic UV-induced invasive cSCCs (n=162). In 39% of the TMAs (n=63) immunohistological stainings unveiled clear colocalization of laminin γ2 chain, p-Smad2 and p-ERK1/2 in tumor cell nuclei located the invasive front of the carcinomas (Fig. 7A). Moreover, in 62% of the cases (n=100), laminin-332 γ2 chain colocalized with p-Smad2. These results demonstrate the concurrent activation of TGF-β and MAPK pathways in cSCCs *in vivo*, and together with experimental evidence presented in this paper strongly suggest that concomitant activation of the two pathways leads to laminin-332 accumulation in the invasive front of the cSCC tumors.

The colocalization of laminin γ2 chain, p-Smad2 and p-ERK1/2 was also examined *in vivo* in a xenograft model in which metastatic cSCC tumor cells (UT-SCC-7) were implanted subcutaneously into the back of severe combined immunodeficient (SCID) mice (n=8). Immunohistological analysis of the xenografts showed that p-ERK1/2 was detected predominantly in the cell nuclei in the invasive front of the tumors, however p-Smad2 and laminin γ2 localized uniformly in the tumor sample, also

386 in fibroblasts (Supplementary Fig. 7). Thus, despite the fact that all eight xenografts contained areas
387 with clear colocalization of laminin γ2 chain, p-Smad2 and p-ERK1/2, the mouse model also had
388 obvious differences when compared to human cSCC tumors.

389
390
391 In conclusion, we report that in cSCC tumors cancer cells that are localized in the invasive front often
392 overexpress laminin-332. The same cells may contain elevated levels of p-ERK1/2 and p-Smad2,
393 proposing that active Ras and TGF-β signaling pathways can also co-operate *in vivo*. Based on a 3D
394 spheroid model and cocultures of skin fibroblasts and various HaCaT-derived active H-Ras
395 harbouring epithelial cells, we have unveiled one mechanism that explains this tissue level
396 phenomenon (Fig. 7B). Firstly, active H-Ras promotes laminin-332 accumulation, and, secondly, also
397 the activation of TGF-β signaling in cancer cells by fibroblasts is required. Together, the same
398 mechanisms are shown to promote cancer cell invasion.

Figure 7

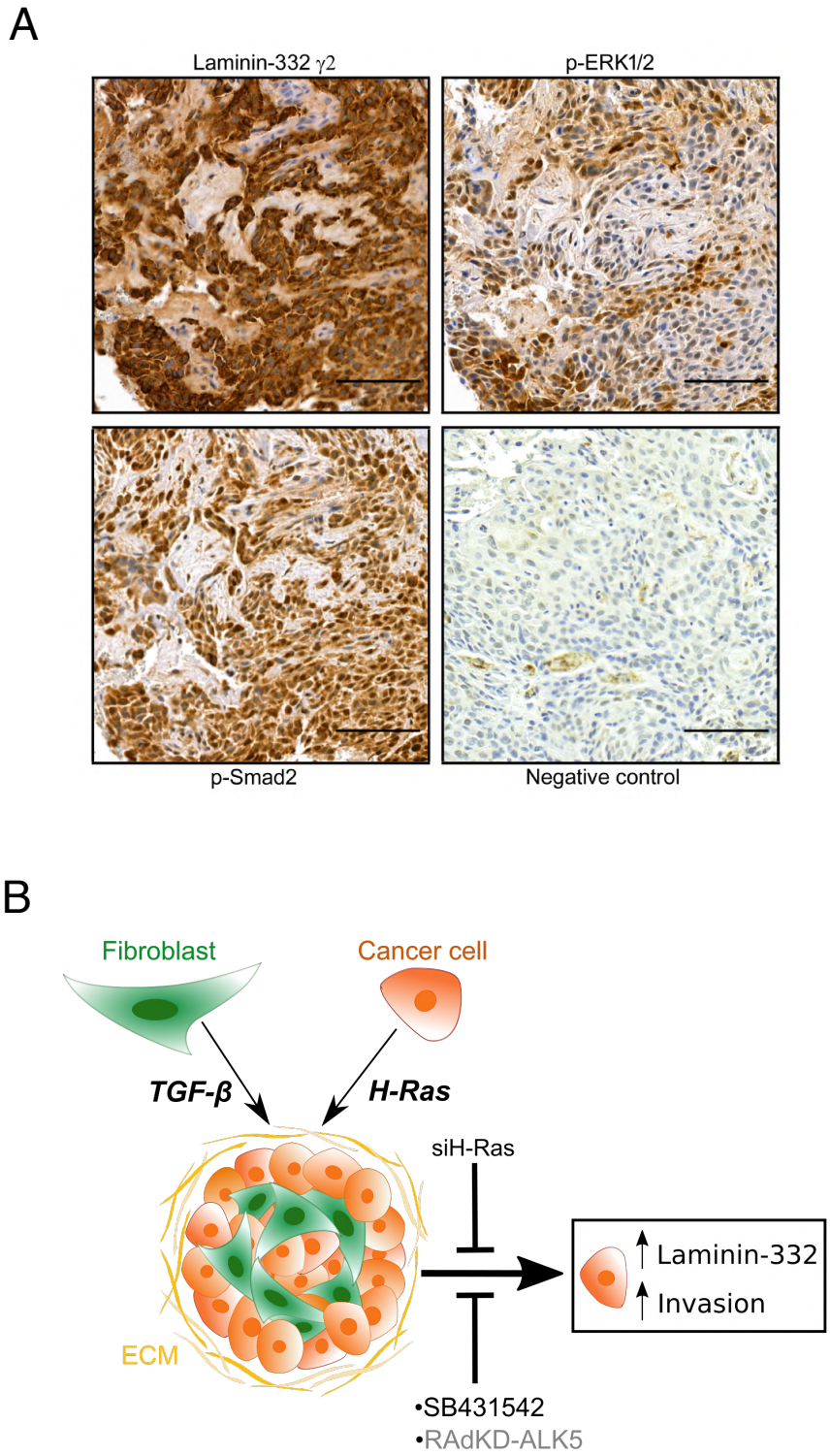

Figure 7. TGF-β and Ras signaling pathways co-operate to induce laminin-332 synthesis in cancer cells. (A) Tissue microarray sections of UV-induced sporadic cSCCs show colocalization of laminin-332 γ2 chain, p-ERK1/2 and p-Smad2 in the invasive edge of the tumors. (B) A model of fibroblast-induced laminin-332 accumulation and cancer cell invasion. Fibroblasts secrete TGF-β, which co-operates with hyperactive H-Ras signaling in 3D spheroids. As an outcome, laminin-332 synthesis increases in cancer cells, promoting cancer cell invasion. This can be blocked either by knocking down H-Ras signaling (siH-Ras), or by inhibiting TGF-β receptor activation by SB431542. *In gray*: kinase-defective adenovirus RAdKD-ALK5 was shown to block laminin-332 accumulation in 3D spheroids harbouring active H-Ras.

DISCUSSION

Laminin-332 is a major protein component in skin basement membrane (BM). Basal keratinocytes use integrin type adhesion receptors, namely α6β4 and α3β1 heterodimers, in anchorage to this laminin in the *lamina rara* layer of BM [16]. Furthermore, laminin-332 also binds to anchoring fibrils formed by collagen VII [37], and it is also found deeper in the dermis in the anchoring plaques [38]. In cSCCs normal BM structures disappear, potentially due to the increased proteolytic activity. Importantly, degradation of BM proteins, including laminins, collagen IV and collagen XVIII, can produce biologically active peptides that are known to promote cell invasion but also inhibit angiogenesis [39], [40], [41], [42].

In various tumor types, including epidermal keratinocyte-derived cutaneous squamous cell carcinoma, laminin-332 is highly expressed and the expression correlates with tumor invasiveness and poor prognosis [16], [17], [40], [43], [44]. Laminin-332 is composed of α3, β3 and γ2 chains, of which γ2 chain is the most intensively studied. Immunohistochemical analyses have shown that its production correlates with metastasis and poor patient survival, and it is often expressed in the invasive front of the carcinomas [45], [46], [47]. Although the function of intracellular laminin-332 is unknown, some studies have detected accumulation of cytoplasmic γ2 chain in invasive carcinomas and the lymph node metastasis [48], in colorectal cancer cells forming tumor budding [49] and in mucinous ovarian neoplasms correlating with infiltrative invasion [50]. It is thus possible that the accumulation of laminin-332, especially the γ2 chain, in tumor cell cytoplasm might be prognostic marker for invasive carcinomas.

Since laminin, as well as laminin-derived protein fragments, can promote the invasion of many cancer cell types [51], [52], [53], we found it interesting that laminin-332 was frequently localized in the invasive front of cSCC tumors. There laminin was produced in tumor cells, but not by activated, cancer-associated stromal fibroblasts. Despite the fact that laminin-332 levels were very high in 56% of the tumor samples, in *in vitro* measurements only one out of seven cSCC cell lines showed

remarkably elevated laminin-332 production. Interestingly, the same cell line showed remarkably increased ERK phosphorylation when compared to other cSCC cell lines. Activated Ras GTPases are the major regulators of MAPK pathway and Ras has been found to be mutated in around 11% of cSCCs [3], [19]. Furthermore, recent studies have shown that patients treated with Raf inhibitors frequently develop cSCCs with *RAS* mutations, mostly in *HRAS* [54], [55].

To study the Ras-dependency of laminin-332 production, we used the well-established HaCaT/*ras*-HaCaT human keratinocyte carcinogenesis model. The three retrovirally H-Ras-transformed cell lines (A5, II-4 and RT3) represent benign, invasive and metastatic phenotypes, respectively [20], [21]. However, in these cell lines, when tested in monolayer cultures or in spheroids, laminin-332 production was not significantly elevated in comparison to HaCaT cells. Thus, Ras or ERK activation alone did not explain the strong accumulation of laminin-332 seen in tissue samples.

The localization of laminin-332 in tumor samples made it possible to speculate that fibroblast–cancer cell interaction may be involved in the stimulation of laminin production. This hypothesis could also explain the observation that only one out of seven cSCC cell lines showed remarkably elevated laminin-332 synthesis in cell cultures. To test this idea, we established 3D spheroids containing both HaCaT/*ras*-HaCaT cells and human skin fibroblasts. In this model, significant increase in laminin-332 production in A5/fibroblasts, II-4/fibroblasts and RT3/fibroblasts cocultures was noted. The most prominent increase was detected in the metastatic RT3 cell line.

Fibroblasts may influence on other cell types in tumor stroma by secreting soluble proteins, such as growth factors, by direct cellular contacts with cancer cells, or by remodeling the ECM [56], [57]. Here, we were able to demonstrate that fibroblast-associated activation of TGF-β signaling and activated Ras/MAPK pathway in cancer cells co-operate in the induction of laminin-332 production in cancer cells and consequently increase cancer cell invasion through collagen I. The previous reports have shown an association between the TGF-β/Smad signaling pathway and the cancer cell invasion and metastasis in cSCC [58], although at the early phases of the malignant process TGF-β

may function as a tumor suppressor [59], [60]. In other cancer types, for example prostate cancer and breast cancer, co-operation of TGF-β and Ras signaling have been suggested to contribute to the progression of disease by stimulating cancer cell proliferation [61] or promoting cell migration [62]. Here, we show that laminin-332 accumulation is critically dependent on both H-Ras and TGF-β/Smad signaling pathways, since H-Ras silencing in RT3 cells totally abolished laminin-332 synthesis, regardless of fibroblast-stimulated TGF-β signaling. Furthermore, when TGF-β receptor activity was blocked by a small molecule inhibitor SB431542 or by kinase-defective RAdKD-ALK5 adenoviral infection, laminin-332 synthesis was not elevated, regardless of activated H-Ras signaling. Interestingly, Ng *et al.* [63] have shown that fibroblast-derived matrix can trigger the development of aggressive cSCC, and the majority of the differentially expressed matrix genes are direct or indirect targets of TGF-β signaling [63]. Thus, scattered information about cSCC progression through hyperactive Ras and TGF-β signaling pathways exist, but the involvement of these pathways for rapid progression and metastatic capacity of cSCC has still remained unclear. Previously, Zapatka *et al*. [64] have reported that laminin-332 production is induced by TGF-β in human colorectal and pancreatic tumor cells, since all three laminin-332 genes (*LAMA3*, *LAMB3* and *LAMC2*) are under positive transcriptional regulation of Smad4 [64]. Interestingly, *KRAS* and *BRAF* are among the most commonly mutated genes in colorectal carcinoma [65] and around 93% of pancreatic ductal adenocarcinomas carry an activating mutation in *KRAS* [66]. It is thus possible to speculate that TGF-β and hyperactive Ras/MAPK signaling pathways are a common duo in regulating laminin-332 accumulation and cell invasion in cancer.

In summary, we show that laminin-332 is expressed *in vivo* in invasive cSCC, mainly in the invasive front of the tumors. We found out that fibroblast-activated TGF-β signaling promotes laminin-332 accumulation in cancer cells in an activated H-Ras-dependent manner, which consequently increases cancer cell invasion. The activation of TGF-β and Ras signaling pathways, and consequent increase in laminin-332 levels was also detected *in vivo* in the invasive front of the cSCC tumors. Our results

provide compelling evidence that fibroblasts have an integral role in the progression of metastatic cSCC, thus highlighting the importance of stromal compartments as therapeutic targets in malignant tumors.

MATERIALS AND METHODS

Ethical issues

Approval for the use of archival tissue specimens of primary cSCCs was obtained from the Ethics Committee of the Hospital District of the Southwest Finland, Turku, Finland. The study was performed in accordance with the Declaration of Helsinki Principles and with the approval of Turku University Hospital. Written informed consent of all participants was obtained before surgery. All the methods used in this study were carried out in accordance with the relevant guidelines and regulations. The experiments with mice were performed with the permission of the State Provincial Office of Southern Finland, according to institutional guidelines (ESAVI/4623/04.10.07/2017).

Cell lines and cell culture

cSCC cell lines were established from surgically removed cSCCs of the skin in Turku University Hospital [67]. Four cSCC cell lines were derived from primary cSCCs (UT-SCC-118, UT-SCC-12A, UT-SCC-105 and UT-SCC-91) and three from metastatic cSCCs (UT-SCC-7, UT-SCC-59A and UT-SCC-115). Cell lines have been authenticated by short tandem repeat DNA profiling (DDC Medical, Fairfield, OH) [68]. The spontaneously immortalized non-tumorigenic human keratinocyte-derived cell line HaCaT [20] and three H-Ras-transformed tumorigenic HaCaT cell lines (A5, II-4 and RT3) [21] were kindly provided by Dr. Norbert Fusenig (German Cancer Research Center, Heidelberg, Germany). Primary adult skin fibroblasts were from the cell line collection of the Medical Biochemistry / the University of Turku and a kind gift from professor Risto Penttinen. The fibroblasts were from male donors aged 18, 19 and 33 years. The fibroblasts were used up to passage number 16.

All cell lines were grown in Dulbecco's modified Eagle's medium (DMEM) supplemented with 10% fetal calf serum (FCS), L-glutamine (6 nmol/L), penicillin (100 U/ml) and streptomycin (100 μg/ml). 1 x MEM non-essential amino acids (11140-035, Gibco) were added to cSCC medium. Geneticin-418 (200 μg/ml) was added to the medium of the H-Ras-transformed cell lines. All cell lines were

routinely tested to be negative for mycoplasma contamination using MycoAlert PLUS Mycoplasma Detection Kit (Cat.No. LT07-710, Lonza).

Tissue samples

Altogether 208 archival formalin-fixed paraffin-embedded tissue samples from sporadic, UV-induced cSCCs were obtained from the archives of the Auria Biobank, Turku University Hospital and the University of Turku and from the archives of the Department of Pathology, Turku University Hospital.

Immunohistochemistry (IHC)

The TMA sections of human cSCC tumors were stained with mouse monoclonal laminin γ2 (1:100; sc-28330, Santa Cruz Biotechnology Inc.), α-Smooth Muscle Actin (1:500; MAB1420, R&D Systems), phospho-p44/42 MAPK (1:400, #4370, Cell Signaling Technology) and phospho-Smad2 (1:2000, #44-244G, Thermo Fisher Scientific) antibodies [14]. Immunostainings were performed in Core Facilities of the Institute of Biomedicine, University of Turku as previously described [69], [70], [71]. The immunostaining of laminin γ2 was scored as negative, weak, moderate, or strong, based on the intensity of cytoplasmic staining. The TMA slides of cSCC samples were digitally scanned using a Pannoramic 250 Slide Scanner or a Pannoramic 1000 Slide Scanner (3DHistech, Budapest, Hungary).

Human cSCC Xenografts

Human cSCC xenografts (n=8) were established as described previously [69]. UT-SCC-7 cells (5×10^6) were injected subcutaneously into the back of severe combined immunodeficiency (SCID/SCID) female mice (CB17/Icr-*Prkdc*^{scid}/IcrIcoCrl) (Charles River Laboratories). Tumors were harvested after 18 days for immunohistochemical analysis.

3D spheroid cultures

For Western blots, confocal imaging and adenoviral assays, 3D spheroids were made in micro-molds according to the manufacturer's instructions (MicroTissues 3D Petri Dish micro-mold spheroids, Sigma-Aldrich) with 2.8×10^5 cells in one mold (8000 cells in one spheroid). In cocultures the cell ratio was 1:2 (HaCaT/*ras*-HaCaT cells and fibroblasts, respectively). In invasion assays, the spheroids contained either 2.5×10^5 cells in one mold (monocultures; 7100 cells/spheroid) or 5.0×10^5 cells in one mold (cocultures; 14 200 cells/spheroid; the cell ratio 1:1). The spheroids were grown in serum-free DMEM medium for three to six days at 37 °C. Ascorbic acid (50 μg/ml) was added daily.

Cell infection with recombinant adenoviruses

Control adenovirus RAd66 [72] was kindly provided by Dr. Gavin W.G. Wilkinson (University of Cardiff, Cardiff, UK), and kinase-defective ALK5 (RAdKD-ALK5) [73] was a kind gift from Dr. Aristidis Moustakas (Ludwig Institute for Cancer Research, Uppsala, Sweden). RT3 cells were infected with a multiplicity of infection (MOI) 100 for 6h in DMEM supplemented with 0.5% FCS. After that, the medium was replaced with fresh DMEM supplemented with 0.5% FCS. On the next day, 3D spheroids were constructed with skin primary fibroblasts and the spheroids were allowed to grow in serum-free DMEM for three days at 37 °C. Ascorbic acid (50 μg/ml) was added daily.

To test the viruses in 2D conditions, RT3 cells were either left uninfected, or infected with RAd66 or RAdKD-ALK5 adenoviruses with MOI 100 for 6h in DMEM supplemented with 0.5% FCS. Thereafter, the medium was replaced with fresh DMEM supplemented with 0.5% FCS and the incubations were continued for 72h. After that, the infected cultures were treated with TGF-β (10 ng/ml) for 30 min at +37 °C, and the cells were harvested in RIPA buffer for Western blot analysis.

CellTracker labeling

HaCaT/*ras*-HaCaT cells and skin primary fibroblasts were labeled with CellTrackers in 2D conditions; HaCaT/*ras*-HaCaT cells in red (CellTracker Orange CMTMR Dye, C2927, Invitrogen)

and fibroblasts in green (CellTracker Green CMFDA Dye, C2925, Invitrogen). The cells were labeled with 2.5 μM dye in DMEM supplemented with 10% FCS for 1h/+37°C, washed twice with PBS and constructed into spheroids. After three to five days, the spheroids were used in invasion assays or fixed for immunofluorescence labeling.

Immunofluorescence

Five-day-old spheroids were fixed with 4% PFA for 1h/+4°C, followed by fixation with 4% PFA supplemented with 1% Triton X-100 for 1h/+4°C. The spheroids were washed twice with PBST (PBS + 0.1% Triton X-100) and blocked with 6% bovine serum albumin in PBST for 5h at room temperature (RT; 20 - 25 °C). Laminin-5 antibody (1:100 in PBST; ab14509, Abcam) was incubated overnight at +4°C, followed by 4h incubation at RT with highly pre-cross absorbed Alexa Fluor 633 goat anti-rabbit IgG secondary antibody (1:200 in PBST; A21071, Invitrogen). The spheroids were mounted in 99% glycerol.

siRNA experiments

The following small inhibitory RNAs (siRNAs) from Eurofins Genomics were used: H-Ras (sense 5' GAACCCUCCUGAUGAGAGU, antisense 5' ACUCUCAUCAGGAGGGUUC), and as a control, nontargeting negative control siRNA (sense 5' UGCGCUAGGCCUCGGUUGC, antisense 5' GCAACCGAGGCCUAGCGCA). ON-TARGETplus SMARTpool siRNAs against human LAMA3 (L-011071-00-0005), human LAMB3 (L-011072-00-0005) and human LAMC2 (L-012119-00-0005) were from Dharmacon RNA Technologies. The cells were transfected with 75 nM siRNAs (in co-transfections, each chain was silenced with 75 nM siRNA) using siLentFect Lipid Reagent (1703361, Bio-Rad) according to the manufacturer's instructions. For 3D spheroid assays, the cells were constructed into spheroids after 24h siRNA transfections and the spheroids were allowed to grow for three days (invasion assays) or five days (Western blots). For 2D assays, the cells were transfected with siRNAs for 72h before harvesting for Western blotting.

584 **Growth factor, cytokine and inhibitor treatments**

585 For growth factor and cytokine stimulations, HaCaT and RT3 cells were first constructed into 3D
586 spheroids and let to grow for 24h in serum-free DMEM. After that, the spheroids were treated for
587 additional 48h with epidermal growth factor (EGF; 20 ng/ml), fibroblast growth factor-2 (FGF-2; 20
588 ng/ml), insulin-like growth factor-I (IGF-I; 20 ng/ml), keratinocyte growth factor (KGF; 20 ng/ml),
589 tumor necrosis factor-α (TNF-α; 10 ng/ml), transforming growth factor-β (TGF-β; 5 ng/ml), vascular
590 endothelial growth factor (VEGF; 20 ng/ml) (all from Sigma-Aldrich), transforming growth factor-α
591 (TGF-α; 5 ng/ml, PeproTech), interferon-γ (IFN-γ; 100 U/ml, Promega) and interleukin-1β (IL-1β;
592 10 ng/ml, Calbiochem), followed by harvesting for Western blotting.

593 For inhibitor treatments, HaCaT and RT3 cells were treated with 10 μM SB431542 (Cat. No. S1067,
594 Selleckhem) and control samples with 0.1% dimethyl sulfoxide (DMSO) in DMEM supplemented
595 with 0.5% FCS for overnight at 37°C. The next day, 3D spheroids were constructed either with or
596 without skin primary fibroblasts and the spheroids were allowed to grow in serum-free DMEM for
597 three days (invasion assays) or for five days (Western blotting). Fresh serum-free medium
598 supplemented with 10 μM SB431542 (or 0.1% DMSO) and ascorbic acid (50 μg/ml) was added daily.
599 To test the inhibitor in 2D conditions, HaCaT and RT3 cells were treated with 10 μM SB431542 (or
600 0.1% DMSO) in DMEM supplemented with 0.5% FCS for overnight at 37°C. After that, the cells
601 were stimulated with TGF-β (10 ng/ml, 30 min/+37°C) and harvested for Western blotting.

602 **Invasion assays from 3D spheroids in collagen I**

603 Before making the spheroids, HaCaT and RT3 cells were treated with hydroxyurea (1 mM in DMEM
604 supplemented with 1% FCS; H8627, Sigma) for 4h at +37 °C to prevent cell proliferation. The cells
605 were then stained with CellTrackers, constructed into spheroids and allowed to grow for three days.
606 Ascorbic acid (50 μg/ml in serum-free DMEM) and hydroxyurea (0.5 mM in serum-free DMEM)
607 were added daily. Three-day-old spheroids were plated on collagen I coated 96-well plates (0.035
608 mg/ml; Collagen solution from bovine skin, C4243, Sigma) and collagen I gel (2.0 mg/ml; Type I

609 Bovine Collagen Solution, 5010, Nutragen) was layered on the top of the spheroids. DMEM
610 supplemented with 10% FCS was added above the collagen gel. To study the effect of TGF-β1
611 receptor kinase inhibitor SB431542 on cell invasion, the medium on top of the collagen I gel was
612 supplemented with 10 μM SB431542, or in control samples with 0.1% DMSO. In the α6 integrin
613 blocking assay, α6 integrin antibody (40 μg/ml) or in control samples, normal rat IgG (40 μg/ml) was
614 added to the medium (DMEM supplemented with 10% FCS) on top of the collagen I gel. Spheroids
615 were allowed to invade for 96h and they were imaged every 24h with Zeiss LSM780 or Zeiss LSM880
616 confocal microscope. Fiji, an image processing platform based on ImageJ [74] was used to calculate
617 the invasion, *i.e.* the area covered by cells. The cell invasion of 2-4 spheroids from each sample were
618 analysed from three independent biological replicates.

619

620 **α6 integrin blocking assay**

621 RT3 cells were first labeled in 2D monolayer cell cultures with red CellTracker for 1h/+37°C, as
622 described above. After that, the cells were detached from tissue culture plastic with 0.025%
623 trypsin/EDTA (Lonza) and incubated with 1 mg/ml trypsin inhibitor (T9128, Sigma-Aldrich) for 5
624 min in suspension. The cells were then centrifuged (4 min/1500 rpm) and resuspended in serum-free
625 DMEM containing function-blocking α6 integrin antibody (40 μg/ml) (CD49f, clone eBioGoH3
626 (GoH3), #14-0495-81, eBioscience) for 1h at 37 °C. In control samples, normal rat IgG (40 μg/ml)
627 (sc-2026, Santa Cruz Biotechnology) was used. The cells were then constructed into spheroids with
628 skin primary fibroblasts (labeled in 2D monolayer cell cultures with green CellTracker) and after
629 three days, the spheroids were used in invasion assays as described above.

630 **Western blot analysis**

631 Samples were harvested in RIPA buffer (89900, Thermo Scientific), separated in 6-13% SDS-
632 polyacrylamide gels and electroblotted onto nitrocellulose membrane (sc-3718, Santa Cruz). The
633 following antibodies were used: laminin-5 (1:1000, ab14509, Abcam); phospho-p44/42 MAPK

(1:1000, #9101), p44/42 MAPK (1:1000, #9102), phospho-Smad2 (1:1000, #3108) and Smad2 (1:1000, #5339) (all from Cell Signaling Technology); H-Ras (1:1000, 18295-I-AP, ProteinTech) and β-actin (1:50 000, A-1978, Sigma-Aldrich).

The membranes were incubated with the primary antibodies overnight at +4 °C, followed by incubation with secondary antibodies (926-32213, 926-32212, 926-68072 or 926-68073, all diluted 1:10 000, LI-COR Biosciences) for 1h/RT. The membranes were scanned with Odyssey infrared imaging system (LI-COR), and the band intensities were determined by densitometric analysis using the Odyssey software. Average from three or four independent biological replicates was calculated.

Mass spectrometry

The proteins from 3D spheroid culture were dissolved in 50 µl of 8 M Urea, 100 mM ammonium bicarbonate. The cysteines were reduced in 10 mM dithiotreitol at 37°C for 1h and alkylated in 40 mM iodoacetamide at room temperature for 1h. LysC/Trypsin mixture (Promega) was added at a 25:1 protein:protease ratio (w/w), and the proteins were digested at 650 rpm at 37°C for 4h. After dilution of the digestion mixture to 0.8 M urea with 100 mM ammonium bicarbonate, the digestion was continued for additional 16h, and subsequently filtrated by a Microcon ultrafiltration device with 10 kDa cutoff (Merck-Millipore, Billerica, MA, USA). The peptides were desalted by StageTips [75] and vacuum dried before the LC-MS/MS run.

An amount of 1 µg of the peptide mixture dissolved in 1 % formic acid at a concentration of 100 ng/µl (determined by absorbance at 280 nm assuming that 1 absorbance unit equals 1 µg/µl) was loaded on a nanoflow HPLC system (Easy-nLC1000, Thermo Fisher Scientific) coupled to the Q Exactive mass spectrometer (Thermo Fisher Scientific) equipped with a nano-electrospray ionization source. The peptides were first loaded on a trapping column and subsequently separated inline on a 15 cm C18 column (75 µm x 15 cm, ReproSil-Pur 5 µm 200 Å C18-AQ, Dr. Maisch HPLC GmbH, Ammerbuch-Entringen, Germany). The mobile phase consisted of 0.1% formic acid (solvent A) and acetonitrile/water (95:5 (v/v)) with 0.1% formic acid (solvent B). The peptides were separated with a

46 min gradient from 7 to 25 % of solvent B followed by 4 min gradient from 25 to 35 % of solvent B. Before the end of the run, the percentage of solvent B was raised to 100 % in 5 min and kept there for 5 min. Full MS scan over the mass-to-charge (m/z) range of 300-1750 with a resolution of 140,000 followed by data dependent acquisition of with an isolation window of 2.0 m/z and a dynamic exclusion time of 30s was performed. The top 10 ions were fragmented by higher energy collisional dissociation (HCD) with a normalized collision energy of 27 and scanned over the m/z range of 200-2000 with a resolution of 17,500. After the MS2 scan for each of the top 10 ions had been obtained, a new full mass spectrum scan was acquired and the process repeated until the end of the 60-min run.

Data analysis for mass spectrometry

Tandem mass spectra were searched using the MaxQuant software (version 1.5.2.8) against a database containing reviewed (SwissProt) human sequences, of UniProtKB release 2017_06. Peptide-spectrum-match- and protein-level false discovery rate thresholds were set to 0.01. Carbamidomethyl (C), as a fixed modification, and oxidation (MKP) as dynamic modifications were included. A maximum of two missed cleavages by trypsin (also before P) was allowed. The LC-MS profiles were aligned (within 20 min), and the identifications were transferred to non-sequenced or non-identified MS features in other LC-MS runs (within 0.7 min). The protein was determined as detected in the sample if its identification had been derived from at least two unique peptide identifications. Filtering for contaminating proteins, reverse identification and identification by site was used. The summed extracted ion intensities of the peptides of each identified protein from three repeated runs of each sample were normalized by the sum of intensities of all identified proteins. The corresponding gene names of all identified proteins along with their log2-transformed normalized intensities were fed to Morpheus tool (https://software.broadinstitute.org/morpheus) and hierarchical clustering of the gene names was performed.

Spheroid intensity profiling

The spheroid intensity profiles obtained from ImageJ were aligned by normalizing the distances from the spheroid edge by spheroid diameter. The original intensity values and spheroid diameter were

685 determined from a single z-stack (the middle stack of all the z-stacks) of confocal images by using
686 the plot profile tool in ImageJ. For each channel separately, the aligned intensities were normalized
687 by the total area under the intensity curve. 12 spheroids from three independent biological replicates
688 were analysed.

689 **Confocal imaging**

690 The spheroids were imaged with Zeiss LSM780 confocal microscope or with Zeiss LSM880
691 AiryScan confocal microscope (Zeiss, Jena, Germany) (10x objective; numerical aperture [NA] 0.3;
692 green CellTracker excitation at 488 nm, orange CellTracker excitation at 543 nm, and Alexa Fluor
693 633-secondary antibody excitation at 633 nm). The imaging was performed at the Cell Imaging Core,
694 Turku Bioscience, University of Turku and Åbo Akademi University.

695 **Statistical analysis**

696 Since it was not possible to estimate the effect size before doing the experiments, initially three
697 independent experiments were performed and the mean and standard deviation of each group were
698 calculated to get the effect size. A program G*power [76] was used to calculate the minimal sample
699 size that ensures power > 80 % to detect the calculated effect size. Sample size of at least three per
700 group was chosen since it ensured power > 80 % in most cases. All quantitative data are presented
701 as mean ± standard deviation (S.D.) or standard error of the mean (S.E.M.), as stated in the figure
702 legends. All data were subjected to the Shapiro Wilk normality test. Levene's test was used to detect
703 the homogeneity of variances between the statistically compared groups. Statistical differences were
704 determined using either analysis of variance (ANOVA) complemented by appropriate post hoc tests
705 (Tukey (variances between the statistically compared groups were similar) or Dunnett's T3 (variances
706 between statistically compared groups were not similar)) or Student's *t*-test. Origin 2015 software
707 (OriginLab Corporation) and SPSS (IBM Corporation, version 25) were used to perform the analyses.
708 Only two-tailed p values < 0.05 were considered as statistically significant. R software version 3.5.1
709 was used to conduct Fisher's exact tests.

ACKNOWLEDGEMENTS

This research was supported by the grants from Jane and Aatos Erkko Foundation, Sigrid Jusélius Foundation, Finnish Cancer Research Foundation and Turku University Hospital (project 13336). We thank the Core Facilities of the Institute of Biomedicine in University of Turku for immunohistochemistry stainings and Auria Biobank in Turku University Hospital and the University of Turku for TMA generation. Maria Tuominen is acknowledged for skillful technical assistance.

AUTHOR CONTRIBUTIONS

J.H. and V-M.K. conceived the project; J.H., V-M.K. and E.S. planned the experiments; E.S. performed the cell experiments, confocal imaging and data analysis; P.R. conducted mass spectrometry experiments and data analysis; P. Riihilä and L.N. planned and generated TMA blocks and planned IHC experiments and analysis. P. Riihilä performed immunohistochemical experiments and data analysis; E.S., J.H. and V-M.K. wrote the manuscript. All authors contributed to manuscript preparation and approved the final version of the manuscript.

DATA AVAILABILITY

The mass spectrometry proteomics data have been deposited to the ProteomeXchange Consortium via the PRIDE [77] partner repository with the dataset identifier PXD013113. Username: reviewer78292@ebi.ac.uk, password: ZQvZiBzd. All other data in this article are available by contacting the corresponding author on reasonable request.

COMPETING INTERESTS

The authors declare no competing interests.

REFERENCES

[1] V. Madan, J.T. Lear, R.-M. Szeimies, Seminar Non-melanoma skin cancer, Lancet. (2016). doi:10.1016/S0140-6736(09)61196-X.

[2] V. Ratushny, M.D. Gober, R. Hick, T.W. Ridky, J.T. Seykora, From keratinocyte to cancer : the pathogenesis and modeling of cutaneous squamous cell carcinoma, J. Clin. Invest. (2012). doi:10.1172/JCI57415.464.

[3] R.J. Cho, L.B. Alexandrov, N.Y. Den Breems, V.S. Atanasova, M. Farshchian, E. Purdom, T.N. Nguyen, C. Coarfa, K. Rajapakshe, M. Prisco, J. Sahu, P. Tassone, E.J. Greenawalt, E.A. Collisson, W. Wu, H. Yao, X. Su, C. Guttmann-Gruber, J.P. Hofbauer, R. Hashmi, I. Fuentes, S.C. Benz, J. Golovato, E.A. Ehli, C.M. Davis, G.E. Davies, K.R. Covington, D.F. Murrell, J.C. Salas-Alanis, F. Palisson, A.L. Bruckner, W. Robinson, C. Has, L. Bruckner-Tuderman, M. Titeux, M.F. Jonkman, E. Rashidghamat, S.M. Lwin, J.E. Mellerio, J.A. McGrath, J.W. Bauer, A. Hovnanian, K.Y. Tsai, A.P. South, APOBEC mutation drives early-onset squamous cell carcinomas in recessive dystrophic epidermolysis bullosa, Sci. Transl. Med. (2018). doi:10.1126/scitranslmed.aas9668.

[4] P. Boukamp, Non-melanoma skin cancer: What drives tumor development and progression?, Carcinogenesis. (2005). doi:10.1093/carcin/bgi123.

[5] E.A. Waterman, N. Sakai, N.T. Nguyen, B.A.J. Horst, D.P. Veitch, C.N. Dey, S. Ortiz-Urda, P.A. Khavari, M.P. Marinkovich, A laminin-collagen complex drives human epidermal carcinogenesis through phosphoinositol-3-kinase activation, Cancer Res. (2007). doi:10.1158/0008-5472.CAN-06-4141.

[6] F. Chen, X. Zhuang, L. Lin, P. Yu, Y. Wang, Y. Shi, G. Hu, Y. Sun, New horizons in tumor microenvironment biology: Challenges and opportunities, BMC Med. (2015). doi:10.1186/s12916-015-0278-7.

[7] D.F. Quail, J.A. Joyce, Microenvironmental regulation of tumor progression and metastasis, Nat. Med. (2013). doi:10.1038/nm.3394.

[8] A. Lujambio, L. Akkari, J. Simon, D. Grace, D.F. Tschaharganeh, J.E. Bolden, Z. Zhao, V. Thapar, J.A. Joyce, V. Krizhanovsky, S.W. Lowe, Non-cell-autonomous tumor suppression by p53, Cell. (2013). doi:10.1016/j.cell.2013.03.020.

[9] K. Shiga, M. Hara, T. Nagasaki, T. Sato, H. Takahashi, H. Takeyama, Cancer-associated fibroblasts: Their characteristics and their roles in tumor growth, Cancers (Basel). (2015). doi:10.3390/cancers7040902.

[10] R. Kalluri, The biology and function of fibroblasts in cancer, Nat. Rev. Cancer. (2016). doi:10.1038/nrc.2016.73.

766 [11] P. Gascard, T.D. Tlsty, Carcinoma-associated fibroblasts: Orchestrating the composition of
767 malignancy, Genes Dev. (2016). doi:10.1101/gad.279737.116.
768 [12] R. Edmondson, J.J. Broglie, A.F. Adcock, L. Yang, Three-Dimensional Cell Culture Systems
769 and Their Applications in Drug Discovery and Cell-Based Biosensors, Assay Drug Dev.
770 Technol. (2014). doi:10.1089/adt.2014.573.
771 [13] M.M. Mueller, W. Peter, M. Mappes, A. Huelsen, H. Steinbauer, P. Boukamp, M.
772 Vaccariello, J. Garlick, N.E. Fusenig, Tumor progression of skin carcinoma cells in vivo
773 promoted by clonal selection, mutagenesis, and autocrine growth regulation by granulocyte
774 colonystimulating factor and granulocyte-macrophage colony-stimulating factor, Am. J.
775 Pathol. (2001). doi:10.1016/S0002-9440(10)62541-2.
776 [14] J.M. Moilanen, S. Löffek, N. Kokkonen, S. Salo, J.P. Väyrynen, T. Hurskainen, A.
777 Manninen, P. Riihilä, R. Heljasvaara, C.W. Franzke, V.M. Kähäri, T. Salo, M.J. Mäkinen, K.
778 Tasanen, Significant role of collagen XVII and integrin β4 in migration and invasion of the
779 less aggressive squamous cell carcinoma cells, Sci. Rep. (2017). doi:10.1038/srep45057.
780 [15] H. Hamasaki, K. Koga, M. Aoki, M. Hamasaki, N. Koshikawa, M. Seiki, H. Iwasaki, J.
781 Nakayama, K. Nabeshima, Expression of laminin 5-γ2 chain in cutaneous squamous cell
782 carcinoma and its role in tumour invasion, Br. J. Cancer. (2011). doi:10.1038/bjc.2011.283.
783 [16] M.P. Marinkovich, Tumour microenvironment: Laminin 332 in squamous-cell carcinoma,
784 Nat. Rev. Cancer. (2007). doi:10.1038/nrc2089.
785 [17] B.G. Kim, H.J. An, S. Kang, Y.P. Choi, M.Q. Gao, H. Park, N.H. Cho, Laminin-332-rich
786 tumor microenvironment for tumor invasion in the interface zone of breast cancer, Am. J.
787 Pathol. (2011). doi:10.1016/j.ajpath.2010.11.028.
788 [18] J. Imura, Y. Uchida, K. Nomoto, K. Ichikawa, S. Tomita, T. Iijima, T. Fujimori, Laminin-5 is
789 a biomarker of invasiveness in cervical adenocarcinoma., Diagn. Pathol. (2012).
790 doi:10.1186/1746-1596-7-105.
791 [19] A.P. South, K.J. Purdie, S.A. Watt, S. Haldenby, N.Y. Den Breems, M. Dimon, S.T. Arron,
792 M.J. Kluk, J.C. Aster, A. McHugh, D.J. Xue, J.H.S. Dayal, K.S. Robinson, S.M.H. Rizvi,
793 C.M. Proby, C.A. Harwood, I.M. Leigh, NOTCH1 mutations occur early during cutaneous
794 squamous cell carcinogenesis, J. Invest. Dermatol. (2014). doi:10.1038/jid.2014.154.
795 [20] P. Boukamp, R.T. Petrussevska, D. Breitkreutz, J. Hornung, A. Markham, N.E. Fusenig,
796 Normal keratinization in a spontaneously immortalized aneuploid human keratinocyte cell
797 line, J. Cell Biol. (1988). doi:10.1083/jcb.106.3.761.
798 [21] P. Boukamp, N.E. Fusenig, E.J. Stanbridge, D. Yin Foo, P.A. Cerutti, c-Ha-ras Oncogene
799 Expression in Immortalized Human Keratinocytes (HaCaT) Alters Growth Potential in Vivo
800 but Lacks Correlation with Malignancy, Cancer Res. (1990).
801 [22] M. Toriseva, R. Ala-aho, S. Peltonen, J. Peltonen, R. Grénman, V.M. Kähäri, Keratinocyte

growth factor induces gene expression signature associated with suppression of malignant phenotype of cutaneous squamous carcinoma cells, PLoS One. (2012). doi:10.1371/journal.pone.0033041.

[23] A. Birgersdotter, R. Sandberg, I. Ernberg, Gene expression perturbation in vitro—A growing case for three-dimensional (3D) culture systems, Semin. Cancer Biol. (2005). doi:10.1016/j.semcancer.2005.06.009.

[24] O. Zschenker, T. Streichert, S. Hehlgans, N. Cordes, Genome-wide gene expression analysis in cancer cells reveals 3D growth to affect ECM and processes associated with cell adhesion but not DNA repair, PLoS One. (2012). doi:10.1371/journal.pone.0034279.

[25] B. Erdogan, D.J. Webb, Cancer-associated fibroblasts modulate growth factor signaling and extracellular matrix remodeling to regulate tumor metastasis, Biochem. Soc. Trans. (2017). doi:10.1042/bst20160387.

[26] B.W. Needleman, J. Choi, A. Burrows-Mezu, J.A. Fontana, Secretion and binding of transforming growth factor β by scleroderma and normal dermal fibroblasts, Arthritis Rheum. (1990). doi:10.1002/art.1780330507.

[27] K. Koli, J. Saharinen, M. Hyytiäinen, C. Penttinen, J. Keski-Oja, Latency, activation, and binding proteins of TGF-β, Microsc. Res. Tech. (2001). doi:10.1002/1097-0029(20010215)52:4<354::AID-JEMT1020>3.0.CO;2-G.

[28] B. Hinz, The extracellular matrix and transforming growth factor-β1: Tale of a strained relationship, Matrix Biol. (2015). doi:10.1016/j.matbio.2015.05.006.

[29] J.S. Munger, D. Sheppard, Cross talk among TGF-β signaling pathways, integrins, and the extracellular matrix, Cold Spring Harb. Perspect. Biol. (2011). doi:10.1101/cshperspect.a005017.

[30] A.G. Stephen, D. Esposito, R.G. Bagni, F. McCormick, Dragging ras back in the ring, Cancer Cell. (2014). doi:10.1016/j.ccr.2014.02.017.

[31] D.K. Simanshu, D. V. Nissley, F. McCormick, RAS Proteins and Their Regulators in Human Disease, Cell. (2017). doi:10.1016/j.cell.2017.06.009.

[32] C.M. Niessen, F. Hogervorst, L.H. Jaspars, A.A. De Melker, G.O. Delwel, E.H.M. Hulsman, I. Kuikman, A. Sonnenberg, The α6β4 integrin is a receptor for both laminin and kalinin, Exp. Cell Res. (1994). doi:10.1006/excr.1994.1099.

[33] A. Sonnenberg, A.A. De Melker, A.M. Martinez De Velasco, H. Janssen, J. Calafat, C.M. Niessen, Formation of hemidesmosomes in cells of a transformed murine mammary tumor cell line and mechanisms involved in adherence of these cells to laminin and kalinin, J. Cell Sci. (1993).

[34] L.M. Shaw, I. Rabinovitz, H.H.F. Wang, A. Toker, A.M. Mercurio, Activation of phosphoinositide 3-OH kinase by the α6β4 integrin promotes carcinoma invasion, Cell.

(1997). doi:10.1016/S0092-8674(00)80486-9.
[35] D. Gambaletta, A. Marchetti, L. Benedetti, A.M. Mercurio, A. Sacchi, R. Falcioni, Cooperative signaling between α6β4 integrin and ErbB-2 receptor is required to promote phosphatidylinositol 3-kinase-dependent invasion, J. Biol. Chem. (2000). doi:10.1074/jbc.275.14.10604.
[36] Z. Cruz-Monserrate, K.L. O'Connor, Integrin α6β4 promotes migration, invasion through Tiam1 upregulation, and subsequent Rac activation, Neoplasia. (2008). doi:10.1593/neo.07868.
[37] R. Brittingham, J. Uitto, A. Fertala, High-affinity binding of the NC1 domain of collagen VII to laminin 5 and collagen IV, Biochem. Biophys. Res. Commun. (2006). doi:10.1016/j.bbrc.2006.03.034.
[38] P. Rousselle, D.R. Keene, F. Ruggiero, M.F. Champliaud, M. Der Van Rest, R.E. Burgeson, Laminin 5 binds the NC-1 domain of type VII collagen, J. Cell Biol. (1997). doi:10.1083/jcb.138.3.719.
[39] K. Miyazaki, Laminin-5 (laminin-332): Unique biological activity and role in tumor growth and invasion, Cancer Sci. (2006). doi:10.1016/j.disc.2005.12.046.
[40] C.M. Guess, V. Quaranta, Defining the role of laminin-332 in carcinoma, Matrix Biol. (2009). doi:10.1016/j.matbio.2009.07.008.
[41] P. Rousselle, K. Beck, Laminin 332 processing impacts cellular behavior, Cell Adhes. Migr. (2013). doi:10.4161/cam.23132.
[42] R. Kalluri, Basement membranes: Structure, assembly and role in tumour angiogenesis, Nat. Rev. Cancer. (2003). doi:10.1038/nrc1094.
[43] P.M. Carpenter, A. Ziogas, E.M. Markham, A.S. Cantillep, R. Yan, H. Anton-Culver, Laminin 332 expression and prognosis in breast Cancer, Hum. Pathol. (2018). doi:10.1016/j.humpath.2018.08.003.
[44] J. Chen, H. Zhang, J. Luo, X. Wu, X. Li, X. Zhao, D. Zhou, S. Yu, Overexpression of α3, β3 and γ2 chains of laminin-332 is associated with poor prognosis in pancreatic ductal adenocarcinoma, Oncol. Lett. (2018). doi:10.3892/ol.2018.8678.
[45] H. Yamamoto, F. Itoh, S. Iku, M. Hosokawa, K. Imai, Expression of the gamma(2) chain of laminin-5 at the invasive front is associated with recurrence and poor prognosis in human esophageal squamous cell carcinoma., Clin. Cancer Res. (2001).
[46] S. Takahashi, T. Hasebe, T. Oda, S. Sasaki, T. Kinoshita, M. Konishi, T. Ochiai, A. Ochiai, Cytoplasmic expression of laminin γ2 chain correlates with postoperative hepatic metastasis and poor prognosis in patients with pancreatic ductal adenocarcinoma, Cancer. (2002). doi:10.1002/cncr.10395.
[47] E.M.R. Silva, V.M. Freitas, W.G. Bautz, L.A.P. de Barros, L.N. da Gama de Souza,

Immunohistochemical Study of Laminin-332 γ2 Chain and MMP-9 in High Risk of Malignant Transformation Oral Lesions and OSCC, J. Oral Maxillofac. Res. (2018). doi:10.5037/jomr.2018.9103.

[48] T. Kainulainen, H. Autio-Harmainen, A. Oikarinen, S. Salo, K. Tryggvason, T. Salo, Altered distribution and synthesis of laminin-5 (kalinin) in oral lichen planus, epithelial dysplasias and squamous cell carcinomas, Br. J. Dermatol. (1997). doi:10.1111/j.1365-2133.1997.tb14938.x.

[49] E. Shinto, H. Mochizuki, H. Ueno, O. Matsubara, J.R. Jass, A novel classification of tumour budding in colorectal cancer based on the presence of cytoplasmic pseudo-fragments around budding foci, Histopathology. (2005). doi:10.1111/j.1365-2559.2005.02162.x.

[50] E. Okuma, Y. Ohishi, Y. Oda, S. Aishima, S. Kurihara, I. Nishimura, M. Yasunaga, H. Kobayashi, N. Wake, M. Tsuneyoshi, Cytoplasmic and stromal expression of laminin γ 2 chain correlates with infiltrative invasion in ovarian mucinous neoplasms of gastro-intestinal type, Oncol. Rep. (2010). doi:10.3892/or-00001019.

[51] G. Giannelli, S. Antonaci, Biological and clinical relevance of Laminin-5 in cancer, Clin. Exp. Metastasis. (2000). doi:10.1023/A:1011879900554.

[52] M. Katayama, N. Sanzen, A. Funakoshi, K. Sekiguchi, Y. Fukushima, Laminin γ2-chain fragment in the circulation: A prognostic indicator of epithelial tumor invasion, Cancer Res. (2003).

[53] K. Miyazaki, J. Oyanagi, A. Sugino, H. Sato, T. Yokose, H. Nakayama, Y. Miyagi, Highly sensitive detection of invasive lung cancer cells by novel antibody against amino-terminal domain of laminin γ2 chain, Cancer Sci. (2016). doi:10.1111/cas.13089.

[54] P.A. Oberholzer, D. Kee, P. Dziunycz, A. Sucker, N. Kamsukom, R. Jones, C. Roden, C.J. Chalk, K. Ardlie, E. Palescandolo, A. Piris, L.E. MacConaill, C. Robert, G.F.L. Hofbauer, G.A. McArthur, D. Schadendorf, L.A. Garraway, RAS mutations are associated with the development of cutaneous squamous cell tumors in patients treated with RAF inhibitors, J. Clin. Oncol. (2012). doi:10.1200/JCO.2011.36.7680.

[55] F. Su, A. Viros, C. Milagre, K. Trunzer, G. Bollag, O. Spleiss, J.S. Reis-Filho, X. Kong, R.C. Koya, K.T. Flaherty, P.B. Chapman, M.J. Kim, R. Hayward, M. Martin, H. Yang, Q. Wang, H. Hilton, J.S. Hang, J. Noe, M. Lambros, F. Geyer, N. Dhomen, I. Niculescu-Duvaz, A. Zambon, D. Niculescu-Duvaz, N. Preece, L. Robert, N.J. Otte, S. Mok, D. Kee, Y. Ma, C. Zhang, G. Habets, E.A. Burton, B. Wong, H. Nguyen, M. Kockx, L. Andries, B. Lestini, K.B. Nolop, R.J. Lee, A.K. Joe, J.L. Troy, R. Gonzalez, T.E. Hutson, I. Puzanov, B. Chmielowski, C.J. Springer, G.A. McArthur, J.A. Sosman, R.S. Lo, A. Ribas, R. Marais, *RAS* Mutations in Cutaneous Squamous-Cell Carcinomas in Patients Treated with BRAF Inhibitors, N. Engl. J. Med. (2012). doi:10.1056/NEJMoa1105358.

[56] A. Östman, M. Augsten, Cancer-associated fibroblasts and tumor growth - bystanders turning into key players, Curr. Opin. Genet. Dev. (2009). doi:10.1016/j.gde.2009.01.003.
[57] T. Marsh, K. Pietras, S.S. McAllister, Fibroblasts as architects of cancer pathogenesis, Biochim. Biophys. Acta - Mol. Basis Dis. (2013). doi:10.1016/j.bbadis.2012.10.013.
[58] S.K. Leivonen, R. Ala-aho, K. Koli, R. Grénman, J. Peltonen, V.M. Kähäri, Activation of Smad signaling enhances collagenase-3 (MMP-13) expression and invasion of head and neck squamous carcinoma cells, Oncogene. (2006). doi:10.1038/sj.onc.1209291.
[59] A.M. Rose, L.C. Spender, C. Stephen, A. Mitchell, W. Rickaby, S. Bray, A.T. Evans, J. Dayal, K.J. Purdie, C.A. Harwood, C.M. Proby, I.M. Leigh, P.J. Coates, G.J. Inman, Reduced SMAD2/3 activation independently predicts increased depth of human cutaneous squamous cell carcinoma, Oncotarget. (2018). doi:10.18632/oncotarget.24545.
[60] P. Cammareri, A.M. Rose, D.F. Vincent, J. Wang, A. Nagano, S. Libertini, R.A. Ridgway, D. Athineos, P.J. Coates, A. McHugh, C. Pourreyron, J.H.S. Dayal, J. Larsson, S. Weidlich, L.C. Spender, G.P. Sapkota, K.J. Purdie, C.M. Proby, C.A. Harwood, I.M. Leigh, H. Clevers, N. Barker, S. Karlsson, C. Pritchard, R. Marais, C. Chelala, A.P. South, O.J. Sansom, G.J. Inman, Inactivation of TGFβ receptors in stem cells drives cutaneous squamous cell carcinoma, Nat. Commun. (2016). doi:10.1038/ncomms12493.
[61] B.J. Park, J. Il Park, D.S. Byun, J.H. Park, S.G. Chi, Mitogenic conversion of transforming growth factor-β1 effect by oncogenic Ha-Ras-induced activation of the mitogen-activated protein kinase signaling pathway in human prostate cancer, Cancer Res. (2000).
[62] E.S. Kim, M.S. Kim, A. Moon, Transforming growth factor (TGF)-β in conjunction with H-ras activation promotes malignant progression of MCF10A breast epithelial cells, Cytokine. (2005). doi:10.1016/j.cyto.2004.10.001.
[63] Y.Z. Ng, C. Pourreyron, J.C. Salas-Alanis, J.H.S. Dayal, R. Cepeda-Valdes, W. Yan, S. Wright, M. Chen, J.D. Fine, F.J. Hogg, J.A. McGrath, D.F. Murrell, I.M. Leigh, E.B. Lane, A.P. South, Fibroblast-derived dermal matrix drives development of aggressive cutaneous squamous cell carcinoma in patients with recessive dystrophic epidermolysis bullosa, Cancer Res. (2012). doi:10.1158/0008-5472.CAN-11-2996.
[64] M. Zapatka, D. Zboralski, Y. Radacz, M. Böckmann, C. Arnold, A. Schöneck, S. Hoppe, A. Tannapfel, W. Schmiegel, P. Simon-Assmann, I. Schwarte-Waldhoff, Basement membrane component laminin-5 is a target of the tumor suppressor Smad4, Oncogene. (2007). doi:10.1038/sj.onc.1209918.
[65] D. Ahmed, P.W. Eide, I.A. Eilertsen, S.A. Danielsen, M. Eknæs, M. Hektoen, G.E. Lind, R.A. Lothe, Epigenetic and genetic features of 24 colon cancer cell lines, Oncogenesis. (2013). doi:10.1038/oncsis.2013.35.
[66] A. V. Biankin, N. Waddell, K.S. Kassahn, M.C. Gingras, L.B. Muthuswamy, A.L. Johns,

D.K. Miller, P.J. Wilson, A.M. Patch, J. Wu, D.K. Chang, M.J. Cowley, B.B. Gardiner, S. Song, I. Harliwong, S. Idrisoglu, C. Nourse, E. Nourbakhsh, S. Manning, S. Wani, M. Gongora, M. Pajic, C.J. Scarlett, A.J. Gill, A. V. Pinho, I. Rooman, M. Anderson, O. Holmes, C. Leonard, D. Taylor, S. Wood, Q. Xu, K. Nones, J.L. Fink, A. Christ, T. Bruxner, N. Cloonan, G. Kolle, F. Newell, M. Pinese, R.S. Mead, J.L. Humphris, W. Kaplan, M.D. Jones, E.K. Colvin, A.M. Nagrial, E.S. Humphrey, A. Chou, V.T. Chin, L.A. Chantrill, A. Mawson, J.S. Samra, J.G. Kench, J.A. Lovell, R.J. Daly, N.D. Merrett, C. Toon, K. Epari, N.Q. Nguyen, A. Barbour, N. Zeps, N. Kakkar, F. Zhao, Y.Q. Wu, M. Wang, D.M. Muzny, W.E. Fisher, F.C. Brunicardi, S.E. Hodges, J.G. Reid, J. Drummond, K. Chang, Y. Han, L.R. Lewis, H. Dinh, C.J. Buhay, T. Beck, L. Timms, M. Sam, K. Begley, A. Brown, D. Pai, A. Panchal, N. Buchner, R. De Borja, R.E. Denroche, C.K. Yung, S. Serra, N. Onetto, D. Mukhopadhyay, M.S. Tsao, P.A. Shaw, G.M. Petersen, S. Gallinger, R.H. Hruban, A. Maitra, C.A. Iacobuzio-Donahue, R.D. Schulick, C.L. Wolfgang, R.A. Morgan, R.T. Lawlor, P. Capelli, V. Corbo, M. Scardoni, G. Tortora, M.A. Tempero, K.M. Mann, N.A. Jenkins, P.A. Perez-Mancera, D.J. Adams, D.A. Largaespada, L.F.A. Wessels, A.G. Rust, L.D. Stein, D.A. Tuveson, N.G. Copeland, E.A. Musgrove, A. Scarpa, J.R. Eshleman, T.J. Hudson, R.L. Sutherland, D.A. Wheeler, J. V. Pearson, J.D. McPherson, R.A. Gibbs, S.M. Grimmond, Pancreatic cancer genomes reveal aberrations in axon guidance pathway genes, Nature. (2012). doi:10.1038/nature11547.

[67] M. Farshchian, A. Kivisaari, R. Ala-Aho, P. Riihil, M. Kallajoki, R. Grénman, J. Peltonen, T. Pihlajaniemi, R. Heljasvaara, V.M. Khri, Serpin peptidase inhibitor clade a member 1 (SerpinA1) is a novel biomarker for progression of cutaneous squamous cell carcinoma, Am. J. Pathol. (2011). doi:10.1016/j.ajpath.2011.05.012.

[68] M. Farshchian, L. Nissinen, V.M. Kähäri, R. Grénman, Dasatinib promotes apoptosis of cutaneous squamous carcinoma cells by regulating activation of ERK1/2, Exp. Dermatol. (2017). doi:10.1111/exd.13109.

[69] P. Riihilä, L. Nissinen, M. Farshchian, M. Kallajoki, A. Kivisaari, S. Meri, R. Grénman, S. Peltonen, J. Peltonen, T. Pihlajaniemi, R. Heljasvaara, V.M. Kähäri, Complement Component C3 and Complement Factor B Promote Growth of Cutaneous Squamous Cell Carcinoma, Am. J. Pathol. (2017). doi:10.1016/j.ajpath.2017.01.006.

[70] P. Riihilä, L. Nissinen, M. Farshchian, A. Kivisaari, R. Ala-aho, M. Kallajoki, R. Grénman, S. Meri, S. Peltonen, J. Peltonen, V.M. Kähäri, Complement factor i promotes progression of cutaneous squamous cell carcinoma, J. Invest. Dermatol. (2015). doi:10.1038/jid.2014.376.

[71] P.M. Riihilä, L.M. Nissinen, R. Ala-Aho, M. Kallajoki, R. Grénman, S. Meri, S. Peltonen, J. Peltonen, V.M. Kähäri, Complement factor H: A biomarker for progression of cutaneous squamous cell carcinoma, J. Invest. Dermatol. (2014). doi:10.1038/jid.2013.346.

[72] G.W.G. Wilkinson, A. Akrigg, Constitutive and enhanced expression from the CMV major IE promoter in a defective adenovirus vector, Nucleic Acids Res. (1992). doi:10.1093/nar/20.9.2233.

[73] M. Fujii, K. Takeda, T. Imamura, H. Aoki, T.K. Sampath, S. Enomoto, M. Kawabata, M. Kato, H. Ichijo, K. Miyazono, Roles of Bone Morphogenetic Protein Type I Receptors and Smad Proteins in Osteoblast and Chondroblast Differentiation, Mol. Biol. Cell. (1999). doi:10.1091/mbc.10.11.3801.

[74] J. Schindelin, I. Arganda-Carreras, E. Frise, V. Kaynig, M. Longair, T. Pietzsch, S. Preibisch, C. Rueden, S. Saalfeld, B. Schmid, J.Y. Tinevez, D.J. White, V. Hartenstein, K. Eliceiri, P. Tomancak, A. Cardona, Fiji: An open-source platform for biological-image analysis, Nat. Methods. (2012). doi:10.1038/nmeth.2019.

[75] J. Rappsilber, Y. Ishihama, M. Mann, Stop And Go Extraction tips for matrix-assisted laser desorption/ionization, nanoelectrospray, and LC/MS sample pretreatment in proteomics, Anal. Chem. (2003). doi:10.1021/ac026117i.

[76] F. Faul, E. Erdfelder, A.-G. Lang, A. Buchner, G*Power 3: a flexible statistical power analysis program for the social, behavioral, and biomedical sciences., Behav. Res. Methods. (2007).

[77] Y. Perez-Riverol, A. Csordas, J. Bai, M. Bernal-Llinares, S. Hewapathirana, D.J. Kundu, A. Inuganti, J. Griss, G. Mayer, M. Eisenacher, E. Pérez, J. Uszkoreit, J. Pfeuffer, T. Sachsenberg, Ş. Yilmaz, S. Tiwary, J. Cox, E. Audain, M. Walzer, A.F. Jarnuczak, T. Ternent, A. Brazma, J.A. Vizcaíno, The PRIDE database and related tools and resources in 2019: Improving support for quantification data, Nucleic Acids Res. (2019). doi:10.1093/nar/gky1106.

SUPPLEMENTARY FIGURES

Supplementary Figure 1

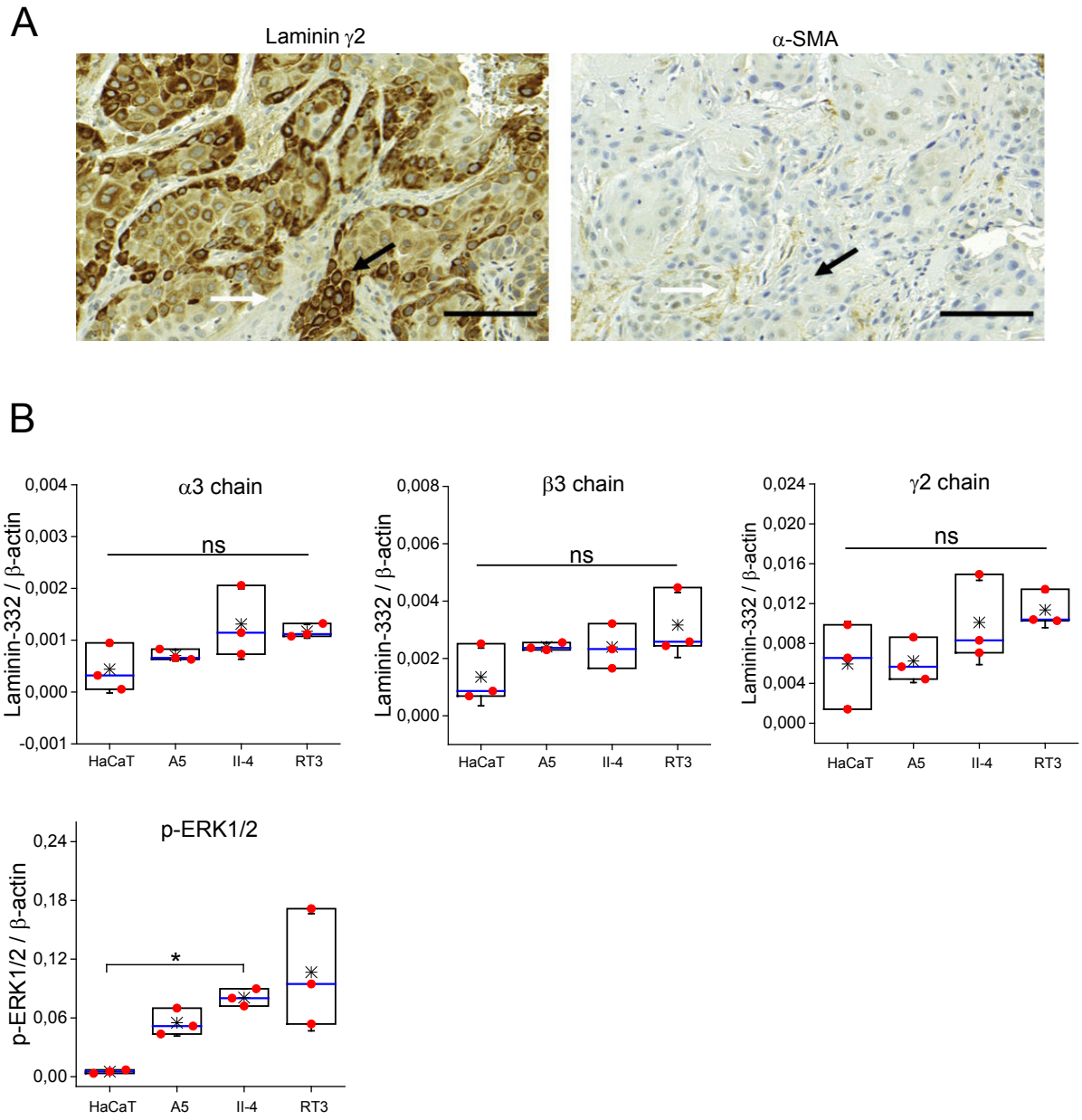

Supplementary Figure 1. Expression of laminin-332 γ2 chain and α-smooth muscle actin (α-SMA) in cSCC tumor samples and laminin-332 in cSCC cell lines and HaCaT/*ras*-HaCaT cells. (A) cSCC tissue section was stained with laminin γ2 antibody (left panel). Specific staining of laminin γ2 was seen in cytoplasm of cSCC tumor cells (black arrow). The surrounding cSCC tumor stroma was negative (white arrow). Parallel tissue section of cSCC was stained with α-SMA antibody (right panel). Specific staining of α-SMA was noted in fibroblasts (white arrow) and the staining of cSCC cells was negative (black arrow). Scale bars=100µm. (B) Quantification of laminin-332 α3, β3 and γ2 chain, and phosphorylated ERK1/2 (p-ERK1/2) from Western blots in Figure 1D. Box plots show data from three independent biological replicates (red dots), the second and third quartiles (the box), the median (blue line) and the mean (star) from all experiments ± S.D. *$p<0.05$, ns=non-significant (one-way ANOVA followed by Tukey or Dunnett's T3 post hoc tests).

Supplementary Figure 2

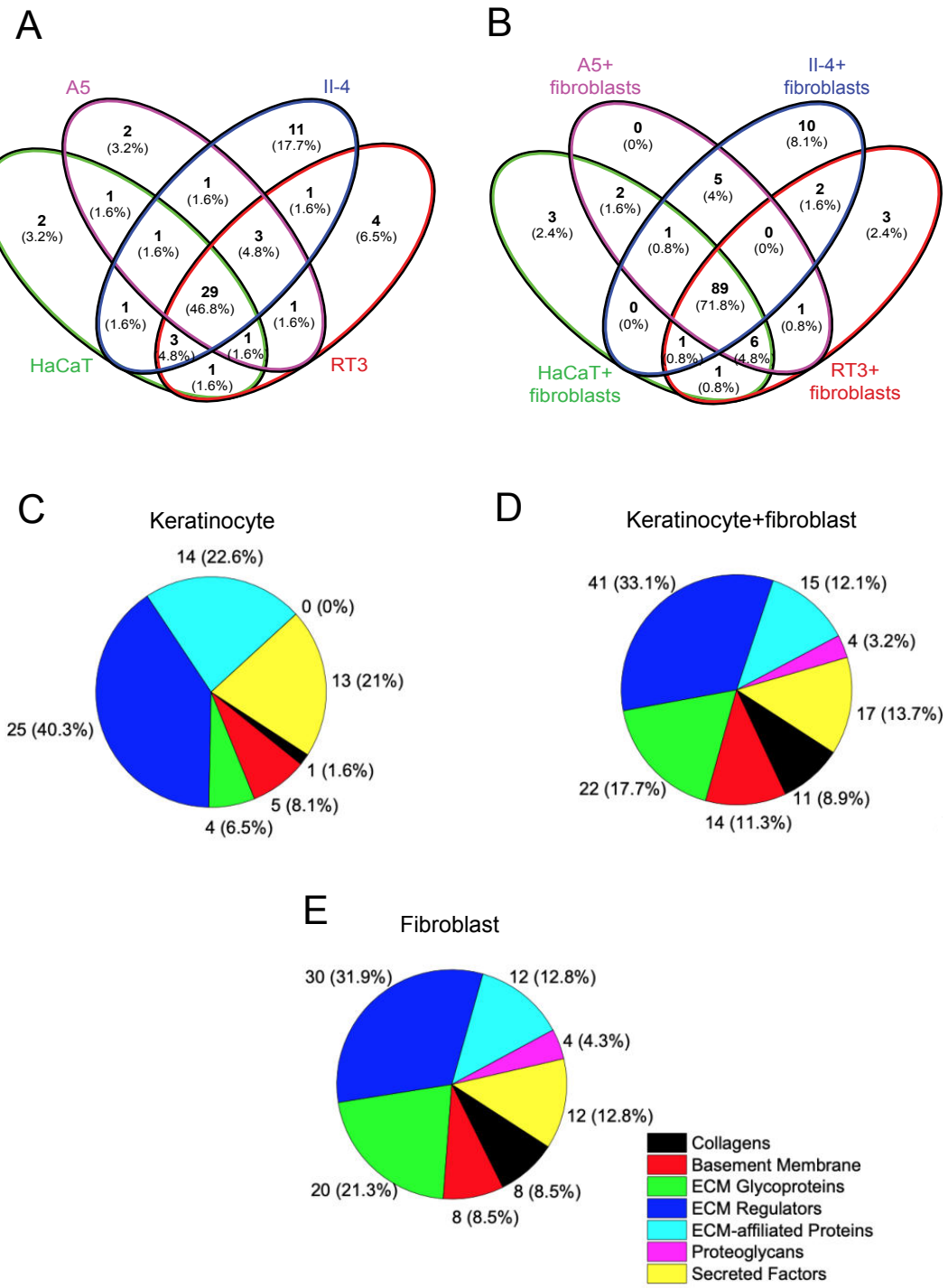

Supplementary Figure 2. Distribution of matrisome proteins among 3D monocultures (HaCaT/*ras*-HaCaT cells alone) and cocultures (HaCaT/*ras*-HaCaT cells with skin primary fibroblasts). (A, B) Venn diagrams show the number and percentage of all detected matrisome proteins when keratinocytes have been cultured alone (A) or as a coculture with fibroblasts (B). (C, D, E) Pie charts show the detected ECM proteins grouped by their ECM categories. (C) Proteins from at least one keratinocyte monoculture (HaCaT, A5, II-4 or RT3). (D) Proteins from at least one keratinocyte coculture with fibroblasts. (E) Proteins from fibroblast monoculture. The protein was regarded as detected if its intensity in the sample was at least 10 times higher than in the blank run and its identification was derived from at least 2 peptide-spectrum matches and transferred peptide identifications.

Supplementary Figure 3

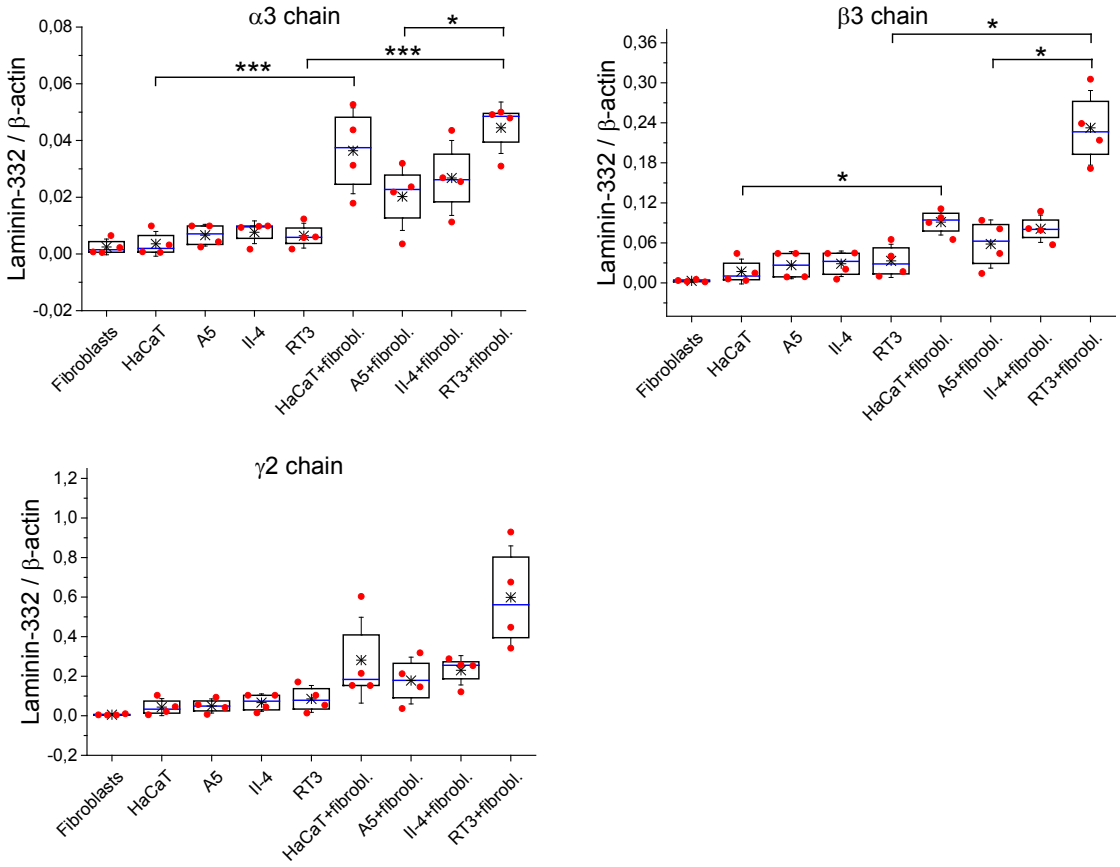

Supplementary Figure 3. Quantification of laminin-332 α3, β3 and γ2 chain from Western blots in Figure 2C. Box plots show data from four independent biological replicates (red dots), the second and third quartiles (the box), the median (blue line) and the mean (star) from all experiments ± S.D. ***$p<0.001$, *$p<0.05$ (one-way ANOVA followed by Tukey or Dunnett's T3 post hoc tests).

Supplementary Figure 4

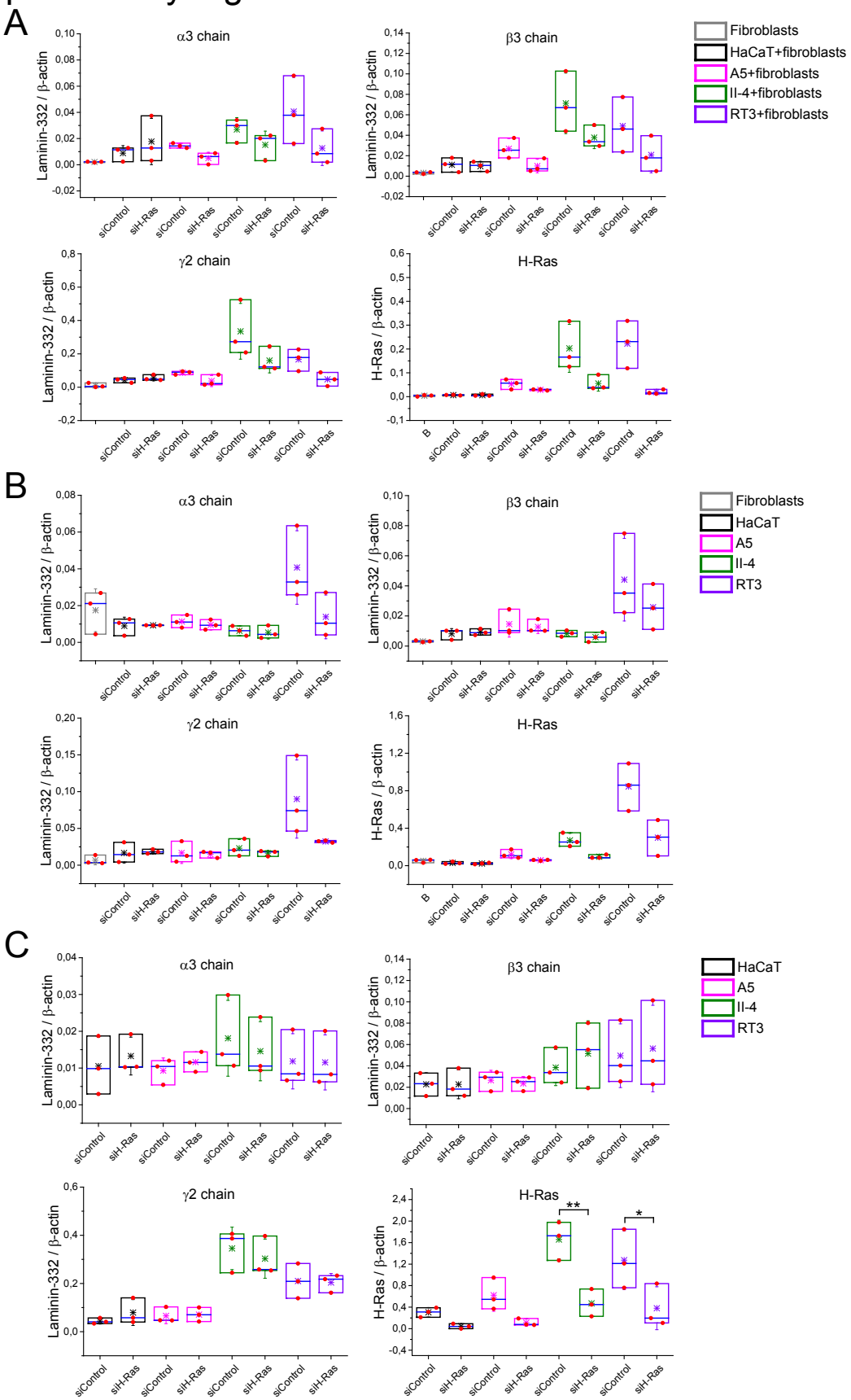

Supplementary Figure 4. Western blot analysis of 3D and 2D cultured HaCaT/*ras*-HaCaT cells after H-Ras silencing. (A) Quantification of laminin-332 α3, β3 and γ2 chain, and H-Ras from Western blots in Figure 3A. Box plots show data from three independent biological replicates (red dots), the second and third quartiles (the box), the median (blue line) and the mean (star) from all experiments ± S.D. (B) Quantification of laminin-332 α3, β3 and γ2 chain, and H-Ras from Western blots in Figure 3B. Box plots show data from three

independent biological replicates (red dots), the second and third quartiles (the box), the median (blue line) and the mean (star) from all experiments ± S.D. (C) Quantification of laminin-332 α3, β3 and γ2 chain, and H-Ras from Western blots in Figure 3C. Box plots show data from three independent biological replicates (red dots), the second and third quartiles (the box), the median (blue line) and the mean (star) from all experiments ± S.D. $**p<0.01$, $*p<0.05$ (one-way ANOVA followed by Tukey post hoc test).

Supplementary Figure 5

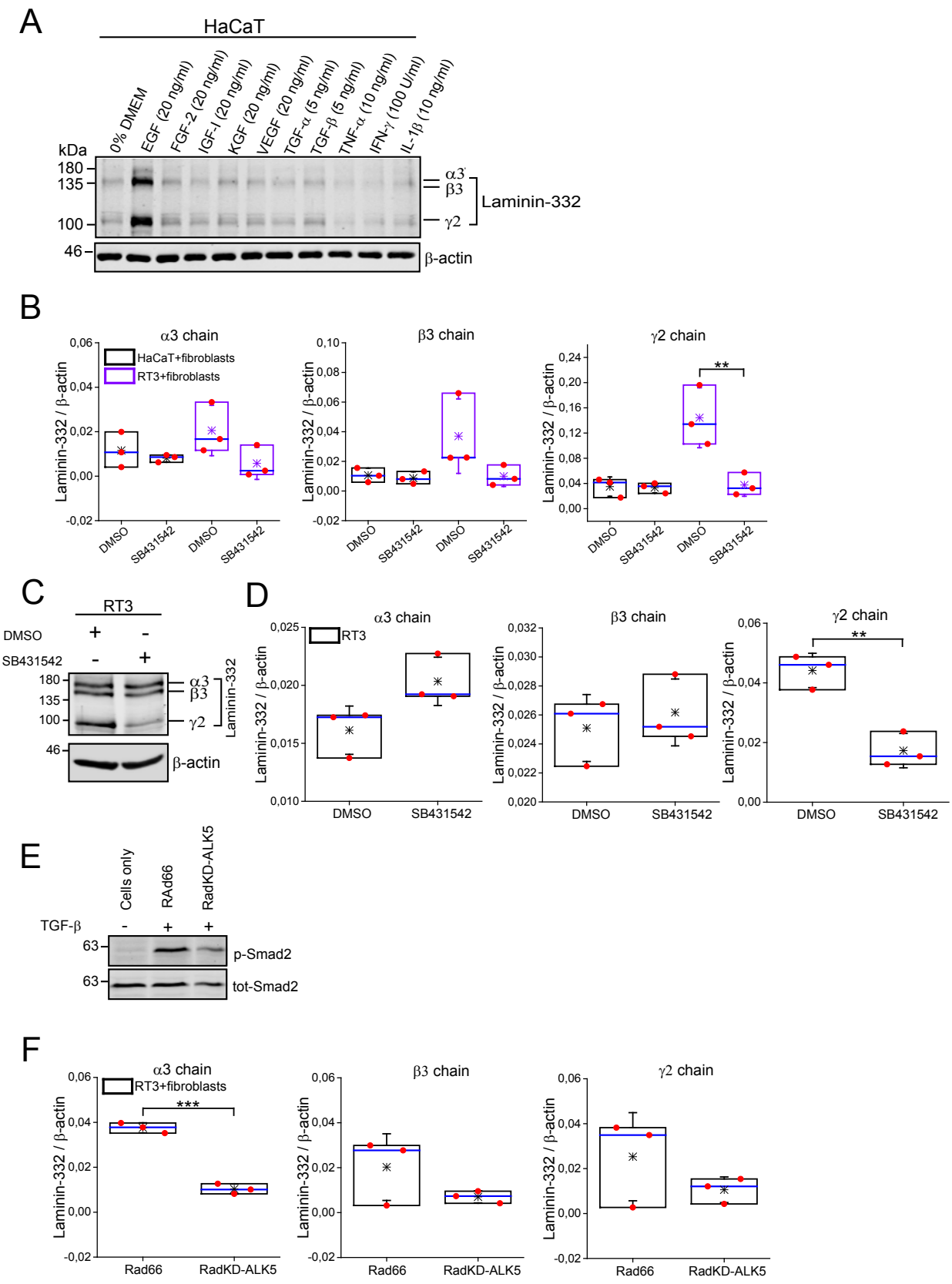

Supplementary Figure 5. Inhibition of fibroblast-derived TGF-β signaling decreases laminin-332 production. (A) Western blot analysis of HaCaT cells that were grown as 3D spheroids for 24h. The spheroids were then subjected to a panel of growth factors and cytokines for additional 48h. β-actin was used as a loading control. (B) Quantification of laminin-332 α3, β3 and γ2 chain from Western blots in Figure 4C. Box plots show data from three independent biological replicates (red dots), the second and third quartiles (the box), the median (blue line) and the mean (star) from all experiments ± S.D. $^{**}p<0.01$ (one-way ANOVA followed by Tukey

post hoc test). (C) RT3 cells were treated with SB431542 or DMSO for 24h, followed by 3D spheroid formation. The spheroids were allowed to grow for five days before harvesting for Western blotting. β-actin was used as a loading control. Representative Western blots from three independent biological replicates are shown. (D) Quantification of laminin-332 α3, β3 and γ2 chain from Western blots in Supplementary Figure 5C. Box plots show data from three independent biological replicates (red dots), the second and third quartiles (the box), the median (blue line) and the mean (star) from all experiments ± S.D. $^{**}p<0.01$ (Student's *t*-test). (E) Western blot analysis of 2D cultured RT3 cells that were either left uninfected or infected (100 MOI) with control adenovirus RAd66 or kinase-defective ALK5 (RAdKD-ALK5) adenovirus for 72h. The cells were then stimulated with TGF-β (10 ng/ml, 30 min/+37°C) and harvested for Western blot analysis for phosphorylated Smad2 (p-Smad2) and total Smad2 (tot-Smad2). (F) Quantification of laminin-332 α3, β3 and γ2 chain from Western blots in Figure 4D. Box plots show data from three independent biological replicates (red dots), the second and third quartiles (the box), the median (blue line) and the mean (star) from all experiments ± S.D. $^{***}p<0.001$ (Student's *t*-test).

Supplementary Figure 6

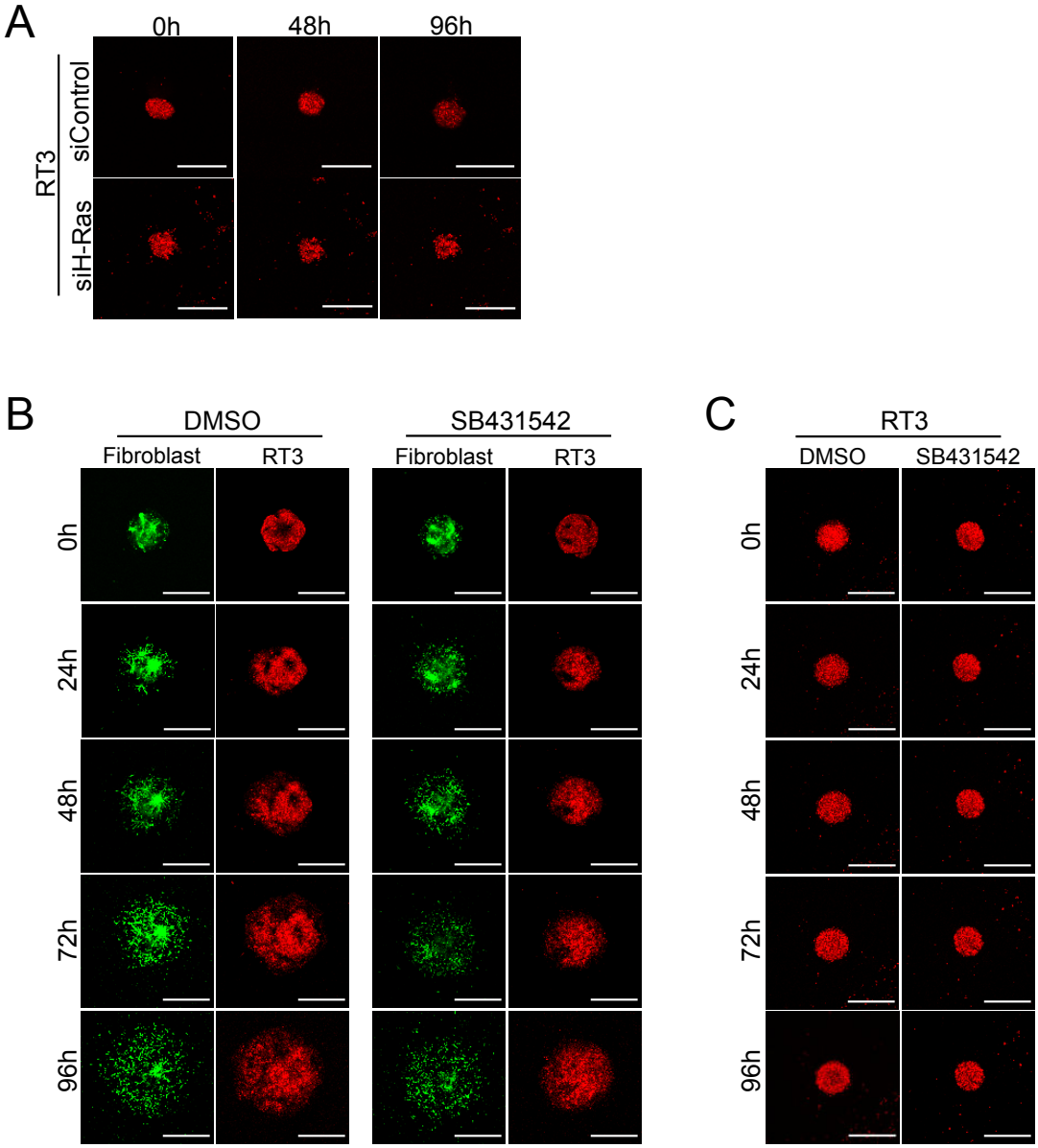

Supplementary Figure 6. RT3 cell invasion through collagen I requires active H-Ras signaling and fibroblast-derived TGF-β signaling. (A) RT3 cells were first treated with H-Ras or control siRNA for 24h, the cells were then labeled with red CellTracker and constructed into 3D spheroids, and allowed to grow for three days. The spheroids were then transferred to a 96-well plate and embedded with a collagen I gel. The invasion was followed by a confocal microscope every 24h during five days. Scale bar, 500 μm. From each time point, 2-4 spheroids were imaged. Three independent biological replicates were performed. (B) RT3 cells were first treated with SB431542 or DMSO for 24h, the cells were then labeled with CellTrackers (RT3 cells in red and fibroblasts in green) and the spheroids were formed with fibroblasts and allowed to grow for three days. After that, the spheroids were transferred to a 96-well plate and embedded with a collagen I gel. The invasion was followed by a confocal microscope every 24h during five days. Scale bar, 500 μm. From each time point, 2-4 spheroids were imaged. Three independent biological replicates were performed. (C) RT3 cells were treated with SB431542 or DMSO for 24h, the cells were then labeled with red CellTracker and constructed into 3D spheroids, and allowed to grow for three days. After that, the spheroids were transferred to a 96-well plate and embedded in a collagen I gel. The invasion was followed by a confocal microscope every 24h during five days. Scale bar, 500 μm. From each time point, 2-4 spheroids were imaged. Three independent biological replicates were performed.

Supplementary Figure 7

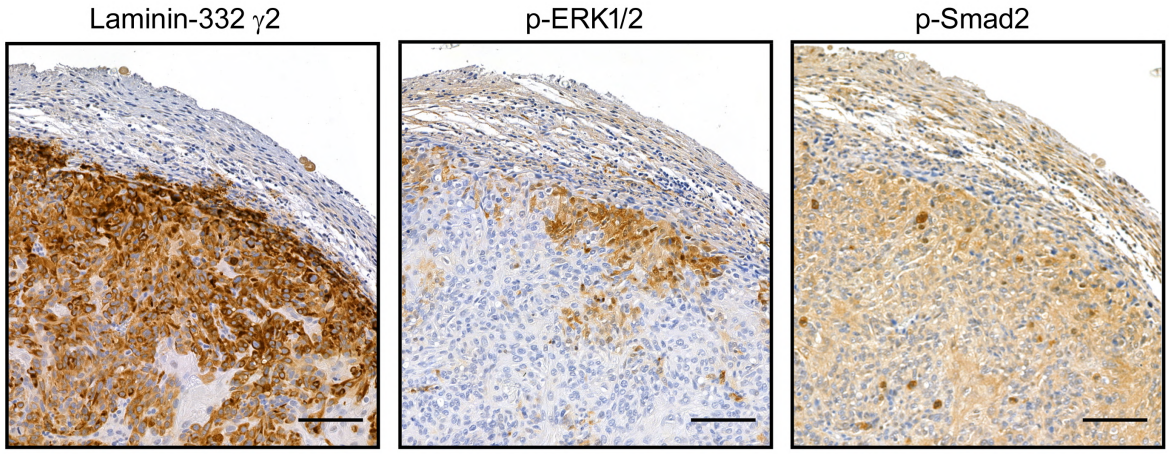

Supplementary Figure 7. Staining of laminin-332 γ2, p-ERK1/2 and p-Smad2 in cutaneous squamous cell carcinoma (cSCC) xenograft tumors. Human metastatic cSCC cells (UT-SCC-7; $5x10^6$) were injected subcutaneously into the back of SCID/SCID mice. Xenograft tumors were harvested after 18 days and stained for immunohistochemistry using laminin-332 γ2 (left panel), p-ERK1/2 (middle panel) and p-Smad2 (right panel) antibodies. The staining for laminin-332 γ2, p-ERK1/2 and p-Smad2 showed colocalization in the xenograft tumor invasive front. Scale bar =100 μm.

Supplementary Figure 8

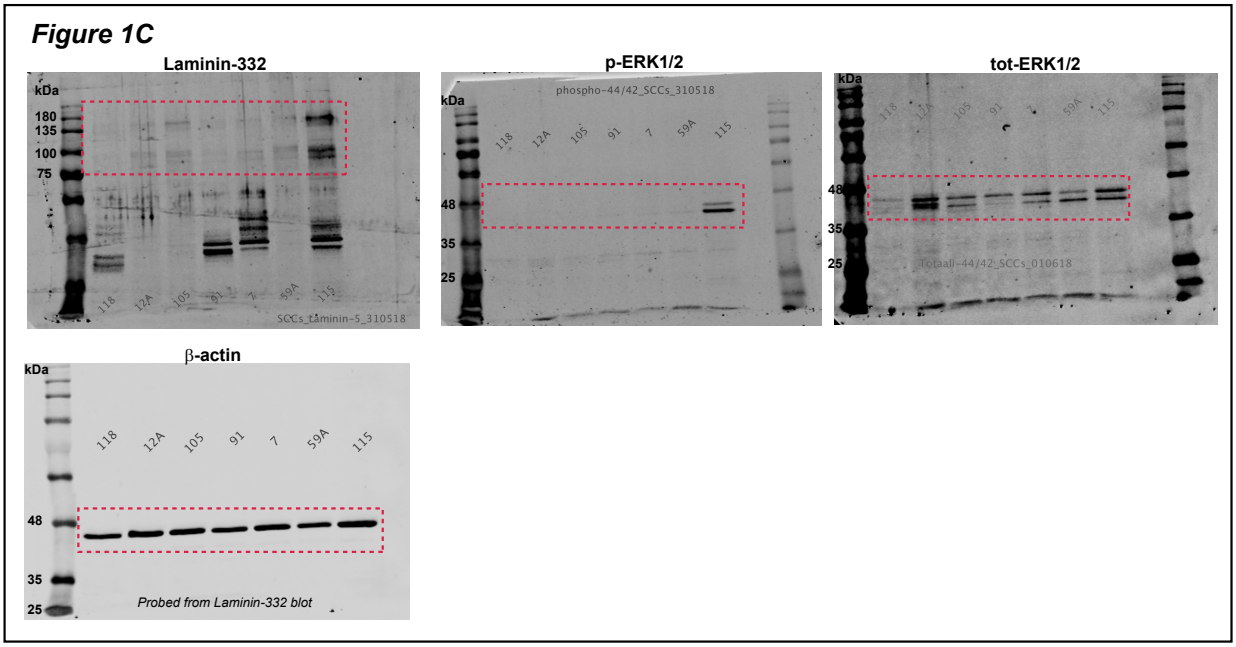

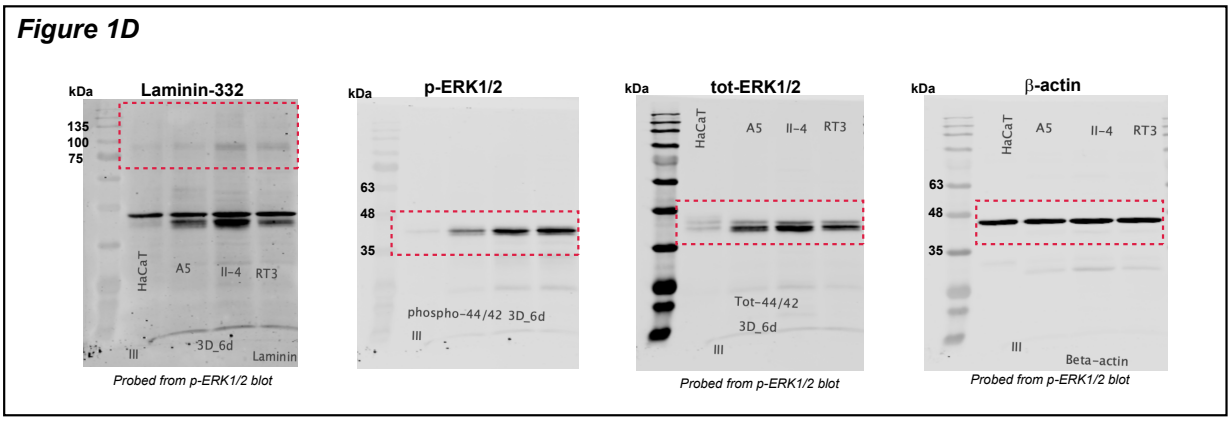

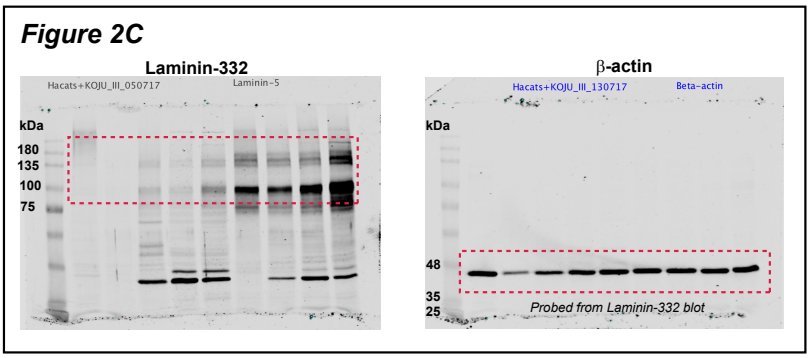

1083

Figure 3A

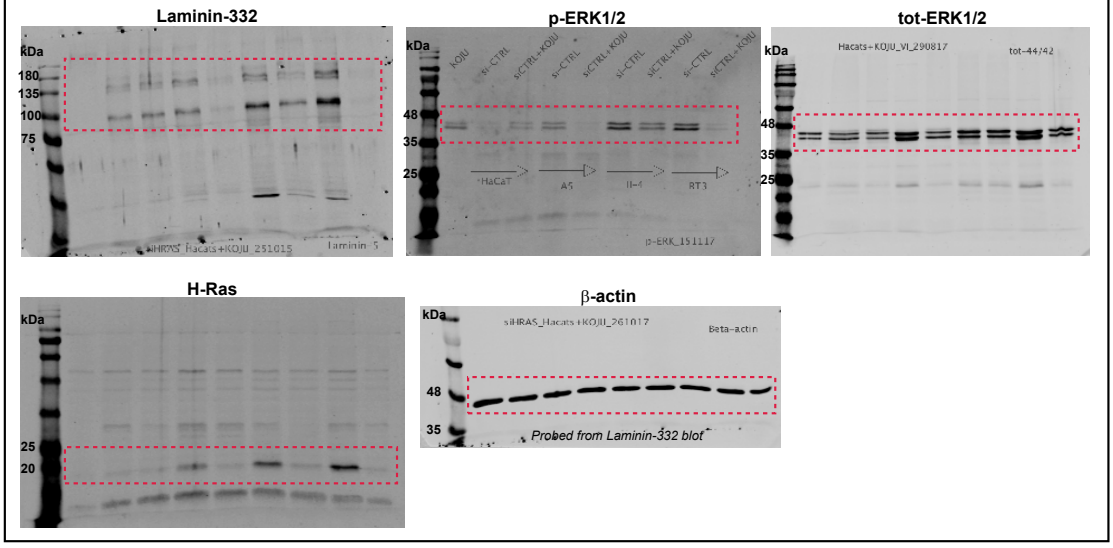

Figure 3B

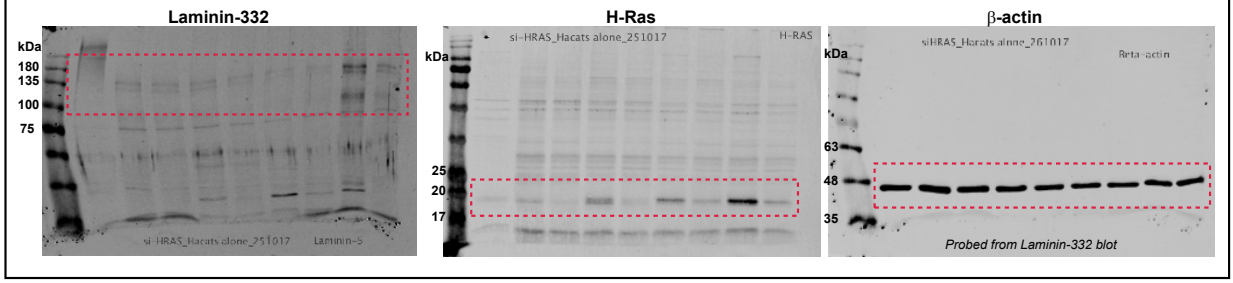

Figure 3C

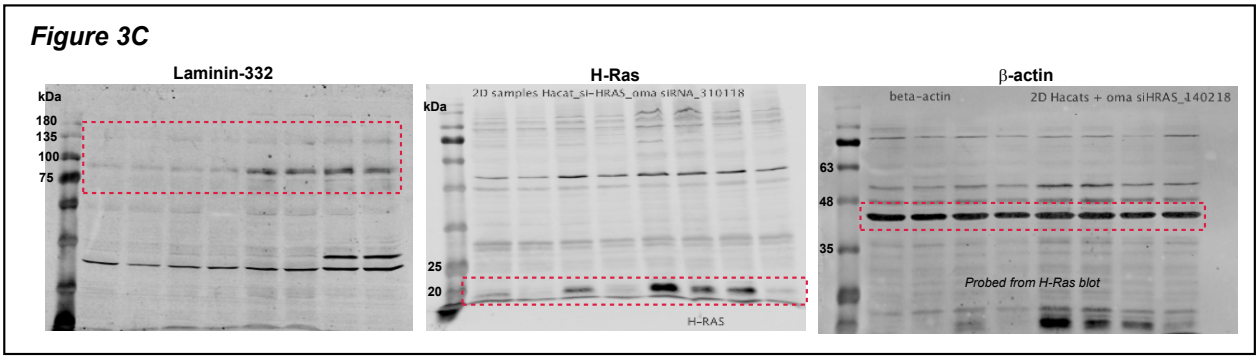

Figure 4A

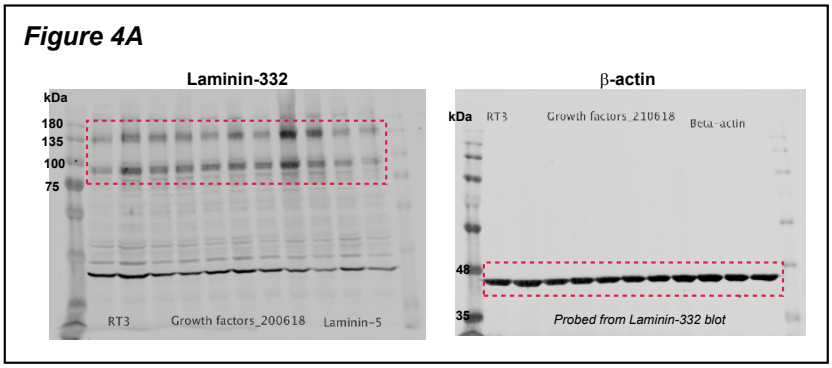

1084

Figure 4B

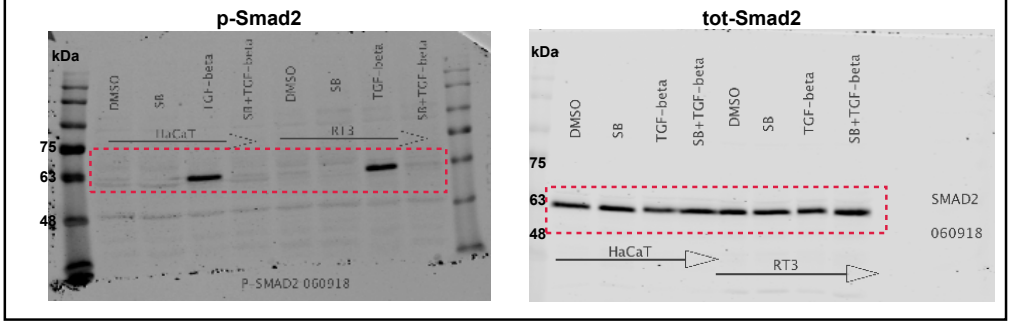

Figure 4C

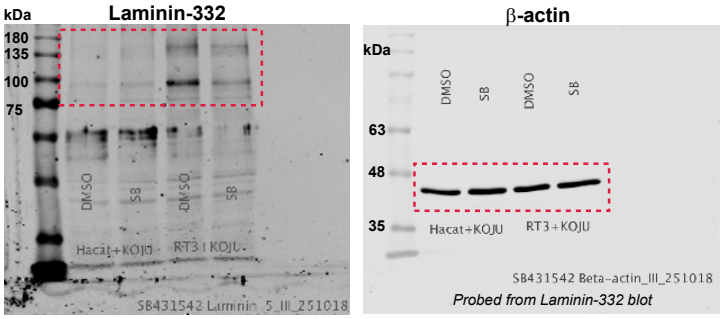

Figure 4D

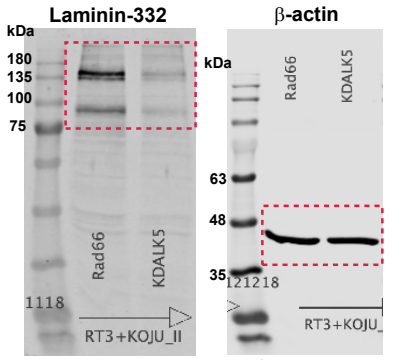

Figure 6A

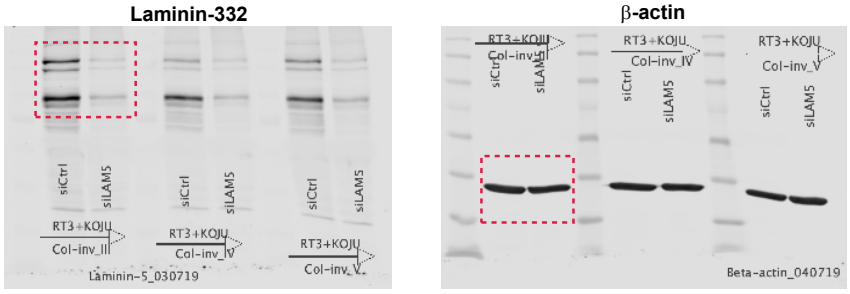

1085

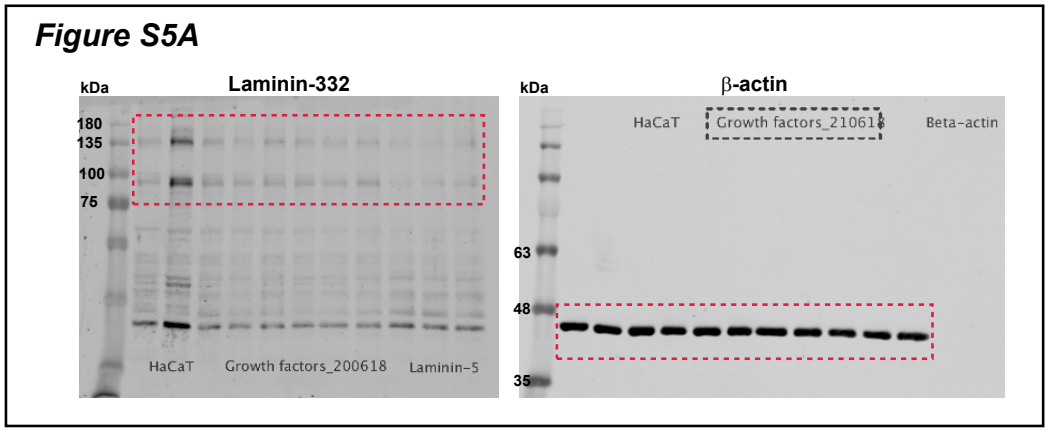

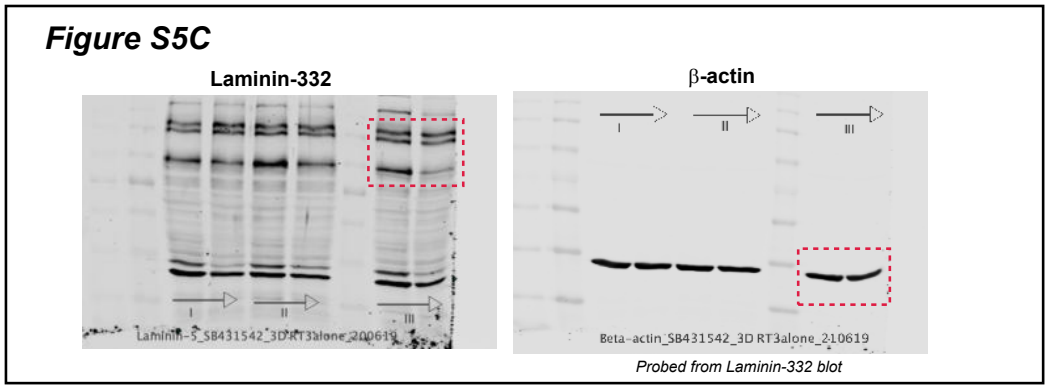

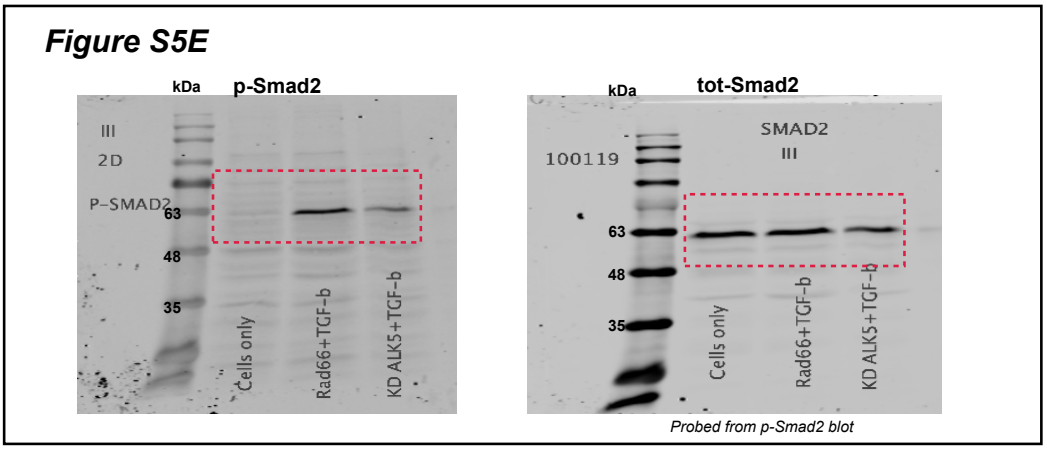

Supplementary Figure 7. Uncropped Western blots from indicated figures in the paper. The red boxes show approximately the cropped parts of the blots presented in the figures.

Supplementary Data 1. Core matrisome and matrisome-associated proteins detected in HaCaT/*ras*-HaCaT cells that were cultured as 3D spheroids either alone or in coculture with skin primary fibroblasts.